Electronic Theses and Dissertations   Theses, Dissertations, and Major Papers

1-1-1992

Ice decay at the base of a supra-ice melt pond.

Emmanuele Mario Novelletto
University of Windsor

Follow this and additional works at: https://scholar.uwindsor.ca/etd

ICE DECAY AT THE BASE OF A SUPRA-ICE MELT POND

by

Emmanuele Mario Novelletto

A Thesis
Submitted to the Faculty of Graduate Studies and Research
Through the Department of Geography
in Partial Fulfilment
of the Requirements for the degree of
Master of Arts
at the University of Windsor

Windsor, Ontario, Canada

1992

UMI Number: EC54836

INFORMATION TO USERS

The quality of this reproduction is dependent upon the quality of the copy submitted.   Broken or indistinct print, colored or poor quality illustrations and photographs, print bleed-through, substandard margins, and improper alignment can adversely affect reproduction.

In the unlikely event that the author did not send a complete manuscript and there are missing pages, these will be noted.   Also, if unauthorized copyright material had to be removed, a note will indicate the deletion.

UMI®

ABSTRACT

ICE DECAY AT THE BASE OF A SUPRA-ICE MELT POND

During the melt season, water accumulates in depressions on sea, lake and river ice, and on glaciers to form ponds. In 1990, a meteorologic and hydrologic study was conducted on two typical supra-ice melt ponds near Resolute, N.W.T., Canada. Field measurements showed that most of the water was isothermal in the convective layer, with temperatures less than 2.6 °C. At the ice-water interface, there was a large temperature gradient and the water was effectively still. The energy balance was dominated by the fluxes of net radiation and sensible heat and consumed almost entirely by melt. The effective thermal diffusivity was found to vary with wind speed and water depth. The heat flux from the water to the ice surface was similar to the results of Lunardini et al. (1986) and could be used to predict melt. The results of this study can be applied to any fresh-water melt pond on ice to predict melt, but because of salinity effects, sea ice ponds may behave somewhat differently.

iv

This Thesis is dedicated to my parents, Egidio and
Filomena Novelletto

v

ACKNOWLEDGEMENTS

I would like to take the opportunity to extend my most sincere appreciation to my academic advisors. First and foremost, I would like to thank Dr. R. Heron for his encouragement, patience, support and professional conduct to what I regard as my most difficult academic challenge. My travel to Resolute Bay N.W.T. during the summer of 1990 will always remain the highlight of my stay at the University of Windsor. To Dr. A. Trenhaile, the departmental reader and Dr. M. Sklash, the external advisor of this thesis, I thank-you for your critical analysis and reading of the thesis. Special thanks also go to Dr. M. Matthew, the chairman of this thesis.

I would also like to acknowledge the departmental support staff (Mrs. J. Belanger, Mrs. M. Clendinning, Mr. R. Kersey, and Mr. R. Welch) for their small but important contribution. In particular, I would like to thank Mr. S. Ecoffier for his computer assistance with the more difficult programs of this thesis.

Last, but certainly not least, I would like to thank my brothers Pietro, Davide and Paolo, Grandmother Rosa, and in particular my mother and father for their emotional support during the most trying times of this thesis.

vi

TABLE OF CONTENTS

3.   OBSERVATIONS AND RESULTS

4.   DISCUSSION AND CONCLUSION

viii

LIST OF TABLES:

LIST OF FIGURES:

NOMENCLATURE:

Upper Case Roman

C_w	heat capacity of water	$J\ m^{-3}\ K^{-1}$
D	exchange coefficient	dimensionless
$D_E,\ D_H$	exchange coefficients	dimensionless
D_G	thermal diffusivity	$m^2\ s^{-1}$
D_m	thermal molecular diffusivity	$m^2\ s^{-1}$
D_s	exchange coefficient	dimensionless
D_u	exchange coefficient	dimensionless
D_w	effective thermal diffusivity	$m^2\ s^{-1}$
F_i	radiation flux reaching the ice-water interface	$W\ m^{-2}$
$K\downarrow$	incoming short-wave radiation	$W\ m^{-2}$
$K\uparrow$	reflected short-wave radiation	$W\ m^{-2}$
L^*	net long-wave flux density	$W\ m^{-2}$
$L\downarrow$	atmospheric long-wave radiation	$W\ m^{-2}$
$L\uparrow$	terrestrial long-wave radiation	$W\ m^{-2}$
L_f	latent heat of fusion	$kg\ m^{-3}$
L_v	latent heat of vaporization	$J\ kg^{-1}$
P	atmospheric pressure	Pa
Q^*	net radiative flux density	$W\ m^{-2}$
Q_A	total absorbed solar radiation	$W\ m^{-2}$

Q_{A1}	radiant energy absorbed in the first pass through the water	$W\ m^{-2}$
Q_{A2}	radiation absorbed following reflection by the water-ice interface	$W\ m^{-2}$
Q_E	latent heat flux density	$W\ m^{-2}$
Q_G	ground heat flux density	$W\ m^{-2}$
Q_H	sensible heat flux density	$W\ m^{-2}$
Q_I	radiation absorbed within an ice layer	$W\ m^{-2}$
Q_{in}	internal heat source per unit volume of water	$W\ m^{-3}$
Q_M	melt energy flux density	$W\ m^{-2}$
Q_P	precipitation heat flux density	$W\ m^{-2}$
ΔQ_S	storage heat flux density	$W\ m^{-2}$
R_a	Rayleigh number	dimensionless
R_i	Richardson number	dimensionless
S_a	specific heat of air	$J\ kg^{-1}\ K^{-1}$
S_i	specific heat of ice	$J\ kg^{-1}\ K^{-1}$
S_w	specific heat of water	$J\ kg^{-1}\ K^{-1}$
T	temperature	K
T_{mn}	temperature of water layer (n) at time (t) and (t-1)	K
T_p	warm plate temperature	$^{\circ}C$
T_w	water temperature	K
T_{ws}	water surface temperature	K
U_a	adjusted wind speed at height z_a	$m\ s^{-1}$

xiv

U_m	measured wind speed at height z_m	m s^{-1}

Lower case Roman

Δh_m	ice surface lowering	m hr^{-1}
ΔT	change in temperature	K
ΔT_R	temperature increase within the ice	K m^{-1}
Δt	change in time or time step increment between current time (n) and next time (n+1)	h
Δz	change in depth	m
Δx	node spacing within ice medium	m
e	emissivity of water surface	dimensionless
e_a	vapour pressure of air	Pa
e_{ws}	vapour pressure of water	Pa
g	acceleration due to gravity	m s^{-1}
h	depth of the fluid layer	m
hi	distance from ice-water interface	m
h_m	ice surface lowering	m
h_n	water layer thickness	m
k	von Kármán constant	dimensionless
k_i	thermal conductivity of the ice medium	W m^{-1} K^{-1}
m	depth node within ice	m
m+1	depth node below m	m
m-1	depth node above m	m

t	time	s
U_a	wind speed at height z_a	m s^{-1}
U_s	surface wind speed	m s^{-1}
z	depth	m
z_a	height above surface	m
z_o	surface roughness parameter	dimensionless

Greek

α_i	albedo water-ice interface	dimensionless
α_w	water surface albedo	dimensionless
β_l	fluid coefficient of expansion of water	°C^{-2}
β_w	fraction of solar radiation transmitted through water surface	dimensionless
τ	Stephan-Boltzman constant	W·m^{-2} K^{-4}
e	ratio of molecular weights of water and air	dimensionless
ρ_l	fluid density	kg m^{-3}
ρ_w	water density	kg m^{-3}
ρ_i	ice density	kg m^{-3}
ϕ	optical extinction coefficient	dimensionless
δ	coefficient	dimensionless

xvi

CHAPTER 1

INTRODUCTION AND LITERATURE REVIEW

1.0 Introduction

The decay of lake, sea and river ice in northern waters is an extremely important annual event. This period marks the beginning of navigation and terminates the use of winter roads and airstrips. The decay period also allows water (river, lake or sea) as well as resident flora and fauna to be exposed to sunshine and oxygen. Hydrologically, the decay of an ice cover is extremely important particularly for operating water management projects.

Unfortunately, the decay of ice is also the time when ice jams cause extensive property damage along river banks and coastlines. The high water and ice levels associated with ice jams may also cause considerable damage to bridge piers, dams and hydroelectric power plants. The risk of navigation is also great during this period. For these reasons, a thorough understanding of the thermal regime of ice covers (river, lake or sea) and the processes involved in their decay is crucial.

1

1.1 Literature Review

1.1.1 The Arctic Melt Season

In the Canadian Arctic Islands, the long and extremely cold winter season leaves this barren landscape snow and ice covered for most of the year. Woo et al. (1981, 1982) claim that the annual Arctic snow cover may persist for at least nine months. Ice thickness studies conducted on lakes, rivers and land-fast sea ice in Canada and Alaska have shown a similar longevity (Bilello, 1980). Hydrologically, the thermal deterioration of the annual arctic snow cover is an important period. It represents the start of the melt season, contributes to the growth and development of a basal ice layer, and aids in the process of ice decay on lakes, rivers, sea and basal ice by forming melt-ponds.

In the Canadian Arctic, snowmelt begins in the Spring when increasing insolation totals raise the mean temperature of the air slightly above 0 °C. Langleben (1966), Woo et al. (1981; 1982), and Woo and Heron (1982) indicate that this phenomenon normally begins between the end of May and June. Initially, snowmelt takes place at the snow-air interface. According to Langham (1981), the mechanisms most responsible for melt at this time are solar radiation absorption and heat transfer by convection to the snow cover. As meltwater is released from the surface, it percolates into the snow cover via capillary and simple gravity drainage (Colbeck 1972;

2

1974). After warming the snow cover, the melt water reaches the ground. In the presence of a cold substrate (-10 to -15 °C), such as lake ice or a frozen ground surface, meltwater reaching this substrate will freeze and a basal ice layer will form (Woo et al., 1981; 1982; Woo and Heron, 1981). Woo and Heron (1981) have found that a basal ice layer may grow to 0.1 m in flat lying areas and 0.25 m in low lying depressions. According to Woo et al. (1981; 1982) a basal ice layer will continue to grow as long as two conditions are satisfied: 1) a sufficient meltwater supply and 2) a subzero substrate. Should the rate of meltwater released by the snow pack exceed the rate of basal ice formation, meltwater will collect at the ice-snow interface (Woo et al. 1982) and run off laterally into low lying areas or depressions (Woo et al. 1982). Supra-ice melt ponds start to appear on lake and sea ice or in depressions when the water level eventually reaches the snow-air interface.

On sea ice, most melt ponds remain throughout the melt period. On lake ice and land surface depressions however, melt ponds have a shorter life span due to a thinner ice cover or drainage. According to some scientists, melt ponds formed on sea ice vary in depth from 0.15 m (Langleben, 1966) to 0.40 m (Untersteiner, 1961). While the horizontal extent of such ponds is difficult to determine in the field, Maykut and Untersteiner (1971) suggest that melt ponds may occupy up to 40 % of the total arctic sea ice area during the summer

3

months.

The existence of melt-ponds on ice is important, for they enhance the melting process by reducing the albedo (reflectivity) of the ice surface and they store radiant energy. Langleben (1968, 1972) for example, has measured the progressive change in the albedo of a air-snow-sea ice situation during the melt season. His findings show that the average albedo value of a fresh snow cover was quite high and near unity. As the snow cover gradually began to melt however, the albedo of the surface decreased to 0.5. A final albedo value of approximately 0.3 was observed as the ice surface deteriorated, forming melt-pools. The gradual reduction in the albedo of a snow or ice surface is of great importance for it allows more solar radiation to be absorbed by the ice medium and in so doing, increases melt. Untersteiner (1961) has observed that the rate of ice melt in ponds that form over sea ice is 2.5 times greater than ice melt rates from bare ice alone. Part of this difference is owing to the storage capacity of melt water ponds. According to Maykut and Untersteiner (1971) a melt-pond with an albedo of 0.3 absorbs an additional 335 MJ m^{-2} of energy compared with a bare ice surface during July and August.

1.1.2 Ice Decay Models

In the scientific literature, researchers have attempted to model ice melt or predict the break-up period in one of two

4

ways. The first method involves the use of statistical relationships employing air temperature records. There are two ways to predict the melt rate or break-up of an ice cover using this method: 1) the melting degree-day method (Ashton, 1983) and 2) the multiple regression equation method (Williams, 1965; 1971; Bilello, 1980). The melting degree-day method attempts to determine the date of break-up by summing the difference between the mean daily temperature and a critical value (0 $^{\circ}$C) until the date of break-up. The results are surprisingly good given that this approach only considers daily air temperature records. For example, Williams (1971) has estimated that the standard deviation for the break-up of 12 continental lakes in Canada lie within a 3.3 to 8 day period.

This approach however does have its limitations, one problem being that the early stages of ice melt are given the same measure of importance as the later stages (Williams, 1971). This is somewhat misleading given that ice melt should be greatest during the later stages as a result of a lower surface albedo and higher radiation totals. A second shortcoming of the melting degree-day method is that it only considers daily air temperature records during the period of ice melt. Williams (1971) claims that the prediction of the decay period of larger lakes could be improved if other variables such as wind and or river flow were included in the procedure.

5

Unlike the melting degree-day method which is based solely upon current air temperature information, the multiple regression technique attempts to determine the date of ice break-up using previous break-up dates and air temperature records. According to Williams (1971), the duration of the melt period is correlated with the deviation of average air temperature during active melt and the average date of start of the melt period. In comparing the melting degree day method to the multiple regression technique, Williams (1971) observed the latter as being more accurate with respect to the estimated date of break-up (standard error 1.6-4.3 days). However, Williams (1971) does note that this method could be improved if other variables such as wind characteristics (fetch, speed, duration, direction), ice thickness and depth of snow cover were included in the analysis.

The second method commonly used by scientists to predict the timing of ice break-up is through the use of energy balance models. Energy balance studies involve the determination of all radiative and energy fluxes involved in the ice melt process. These models are physically based, employing empirical coefficients and parameters related to the physical properties of ice (eg. salinity, density, transmissivity), snow (eg. albedo, thickness, density) and/or water (eg. temperature, heat capacity, optical extinction coefficient). Energy balance methods are more realistic than empirical methods but require more data.

6

Studies of this nature have been found to reasonably predict ice thickness on rivers (Green and Outcalt, 1985), lakes (Rumer and Yu, 1978; Wake and Rumer, 1979) and arctic sea ice (Untersteiner, 1961; Maykut and Untersteiner; 1971). Despite their apparent success, very few models have been designed specifically for northern and sub-arctic lakes (Fox et al., 1979). The most recent energy balance model developed for a high arctic lake ice cover in Canada is that of Heron (1985).

While energy balance studies and air temperature models reasonably represent the timing and rate of ice decay, such models could be improved if the effects of meltwater ponds were considered.

1.1.3 Energy Balance Studies

In the scientific literature, a variety of energy budget studies have been conducted on snow and ice surfaces. Some of these studies were located on glaciers (Braithwaite, 1981; Aver'yanov, 1983; Hay and Fitzharris, 1988; Munro, 1990) while other studies were conducted on sea ice (Untersteiner, 1961; Langleben, 1966; Maykut and Untersteiner, 1971), river ice (Green and Outcalt, 1985) and lake ice (Rumer and Yu, 1978; Wake and Rumer, 1979; Heron, 1985). While the methods and parameters used in each study differed, their common goal was to determine the energy available for ice melt.

The equation commonly used by researchers to determine

the energy available for melting a snow or ice surface is generally expressed as

$$Q_M = Q* + Q_E + Q_H + Q_G + Q_P + \Delta Q_S \qquad \text{(Equation 1)}$$

where Q_M represents the melt energy flux density ($W\ m^{-2}$), $Q*$ is the net radiative flux density ($W\ m^{-2}$), Q_E is the latent heat flux density ($W\ m^{-2}$), Q_H is the sensible heat flux density ($W\ m^{-2}$), Q_G refers to the heat flux penetrating through the ice medium into the ground ($W\ m^{-2}$), Q_P is the heat flux due to precipitation ($W\ m^{-2}$), and ΔQ_S is the change in heat storage (internal) per unit area of snowcover ($W\ m^{-2}$) (Male and Gray, 1981; Oke, 1987). A positive sign indicates energy gained by an interface or layer of material.

The net flux of radiation ($Q*$) is the sum of all incoming and outgoing radiant flux densities and is expressed as

$$Q* = K\downarrow - K\uparrow + L\downarrow - L\uparrow \qquad \text{(Equation 2)}$$

where $K\downarrow$ refers to incoming short-wave (0.15 - 4 μm wavelength) solar radiation ($W\ m^{-2}$), $K\uparrow$ is the reflected short-wave solar radiation ($W\ m^{-2}$), $L\downarrow$ is the incoming (atmospheric) long-wave (> 4 μm) radiation ($W\ m^{-2}$) and $L\uparrow$ refers to the outgoing (terrestrial) long-wave radiation ($W\ m^{-2}$) (Oke, 1987; Arya, 1988). For a snow or ice surface, the net radiative flux density supplies the greatest proportion of energy

8

available for ice melt (Langleben, 1966; Maykut and
Untersteiner, 1971). Hay and Fitzharris (1988) for example,
have concluded that net radiation supplies 52 % of the total
available energy for glacial ice melt. While this total agrees
with earlier studies (Braithwaite, 1981), a recent glacial ice
investigation by Munro (1990) shows that this total may rise
to as high as 65 %.

Sensible heat flux density (Q_H) is defined by Arya (1988)
as the transfer of heat through the process of convection due
to surface and air temperature differences. Glacial and lake
ice studies conducted by Braithwaite (1981), Heron (1985), Hay
and Fitzharris (1988) and Munro (1990) show that Q_H accounts
for between 34 % to 47 % of the total energy available for ice
melt.

Latent heat flux density (Q_E) refers to the amount of
energy released or absorbed when a body changes state and is
the result of evaporation, evapotranspiration or condensation
at the surface (Arya, 1988). The proportion of latent heat
energy used to melt glacial and lake ice is found by some
scientist to vary with respect to climatological conditions.
Munro (1990) estimates that Q_E accounts for 1% of the total
available energy for ice melt while Braithwaite (1981), Hay
and Fitzharris (1988) show that this total may increase to as
high as 12 %. Lake ice decay investigations conducted by
Heron (1985) show that Q_E is responsible for 7 % to 13 % of
total ice melt.

Q_G refers to the conduction of heat energy from the ice or snow surface into the underlying ground or water substrate. Oke (1987) indicates that Q_G may significantly contribute to the ice melt process if the snow layer is thin and a great deal of energy exchange occurs across the base of the snowpack. On glacial ice, these conditions may not exist and hence Q_G is often ignored in the energy budget (Hay and Fitzharris, 1988; Munro, 1990). Braithwaite (1981) however, was able to statistically determine the average percentage of energy conducted into glacial ice (Q_G) from four case studies using linear regression analysis. The results of his analysis show that, on average, approximately 13 % of the total energy available for ice melt enters the ice medium. This energy sink reduces ice melt and raises the overall temperature of the ice medium.

In areas where storms originate over large warm water bodies, the heat flux due to precipitation (Q_P) may provide a significant source of melt energy (Oke, 1987). Where these conditions are not met however, Q_P is small since it does not involve a change of state, and it is often ignored in energy balance studies (Aver'yanov, 1983; Munro, 1990). While difficult to measure in the field, Heron (1985) has observed that the contribution Q_P to the ice melt process is minimal. Energy balance studies conducted on glacial ice by Hay and Fitzharris (1988) show that Q_P may supply approximately 2% of the total energy available for ice melt.

10

Finally, ΔQ_s refers to the change in energy stored within the snow, water or ice cover (Male and Gray, 1981; Oke, 1987). According to Male and Gray (1981), the internal energy of the snow cover consists of components from the solid, liquid and vapour phases of the snow. While suitable methods have been devised to determine the internal energy of a shallow snow cover (Granger and Male, 1978), modelling the thermal regime of a thick, wet, snow cover is very complex (Male and Gray, 1981). This is because of the daily freeze-thaw cycle experienced by the snow cover. While difficult to determine, the magnitude of ΔQ_s is very small (Granger and Male, 1978) and often ignored in energy balance studies (Munro, 1990).

1.1.4 Theory

The presence of a water body over an ice surface can have a considerable influence on the rate of ice melt by absorbing, scattering and reflecting radiation (Viskanta and Toor, 1972). Water also attains a maximum density at 3.98 °C (Ashton, 1986), and numerous laboratory experiments have shown that when temperature differences are found within a water-ice system, the associated density differences create complex cellular-like motions within the water (Townsend, 1964; Musman, 1968; Myrup et al., 1970; Moore and Weiss, 1973; Adrian, 1975; Lunardini et al., 1986). This phenomenon, commonly referred to as natural convection, transfers heat to the water-ice interface and contributes to the ice melt

11

process.

The laboratory experiments performed by Yen (1968, 1980) and Yen and Galea (1969) are the most comprehensive temperature convection studies, for they allowed water layers to form over an ice surface and increase with depth as melt progressed. Their laboratory experiment showed that upon initial ice melt, a stable meltwater region (temperature > 3.98 °C) formed above an unstable region (0 °C < temperature < 3.98 °C) near the water-ice interface. In the absence of convection, they observed a linear water temperature profile and a flat water-ice interface.

The criterion commonly used to determine the significance of natural convection is the Rayleigh number. The Rayleigh number is a dimensionless parameter which represents the time required to heat a fluid layer by conduction, and the time required for fluid particles to circulate once around the convection cell (Whittow, 1984). In its most basic form, the Rayleigh number (R_a) is commonly expressed as

$$R_a = g \ \beta_1 \ \rho_w^2 \ S_w \ h^3 \ \Delta T \ / \ \mu_1 \ k_1 \qquad \text{(Equation 3)}$$

where g represents the acceleration due to gravity (m s^{-2}), β_1, the fluid's coefficient of expansion (K^{-2}), ρ_w, fluid density (kg m^{-2}), C_1, the specific heat of the fluid (J kg^{-1} K^{-1}), h, depth of the fluid layer (m), ΔT, temperature difference across the liquid layer (K), μ_1, fluid viscosity (N s m^{-2}),

12

k_l, fluid thermal conductivity $(W\ m^{-1}\ K^{-1})$ (Yen, 1969; Yen and Galea, 1969).

Yen (1968, 1980) and Yen and Galea (1969) believe that the critical Rayleigh number is not a single value but varies as upper boundary (warm plate) temperature conditions alter. When the warm plate temperature (T_p) lies within 6.72 °C and 25.50 °C, Yen (1968), Yen and Galea (1969) theorize that the critical Rayleigh number (R_c) may be determined from the following empirical equation:

$$R_c = 14,200 \times \exp\ (-6.64 \times 10^{-2}\ T_p) \qquad \text{(Equation 4)}$$

Upon the onset of convection they noticed that the water-ice interface became covered with small, circular, equally spaced concentric ridges. As convection progressed with time, the water-ice interface was transformed into a highly irregular-shaped surface. Their analysis also showed that water temperature profiles deviated from the non-convective linear form. Once a fairly large meltwater region was produced, the researchers noted that convection intensity decreased as a region of constant water temperature (3.21 °C) was established for most of the water column (Yen, 1968; 1980; Yen and Galea; 1969).

Musman (1967) and Adrian (1975) examined the nature of circulation in a layer of water overlying ice and discovered that one or more counter rotating cells formed above and/or

13

beside the principal convection cell. Using a laser-doppler velocimeter, Adrian (1975) empirically determined that the speed of the convection cells is quite small, ranging from 0.04 mm s^{-1} to 0.56 mm s^{-1}. As for the number of cells found in an water-ice complex, Musman (1967) observed that the number of counter rotating cells was dependent upon the magnitude of the Rayleigh number. The number of counter rotating cells decreased from 2 to 1 as the Rayleigh number increased from 2.5 to 12.0. At Rayleigh numbers exceeding 12, Musman (1967) observed a ice-water system dominated by the principal cell.

The laboratory results of Musman (1967), Yen (1968, 1980), Yen and Galea (1969) and Adrian (1975) provide a fairly detailed physical description of the convective process in an ice-water system that is heated from above and cooled from below. These studies may be unrealistic however, because of the high water temperatures created and the rather small confined systems used in the experiments. Therefore their results should be treated with caution.

To date, the most realistic experiment approximating a melt pond was devised by Lunardini et al. (1986). Their goal was to determine the convective heat flux (Q_w) flowing from water to a flat ice substrate. Their study was conducted in a large ice flume where water temperature, ice temperature, water depth, bulk water flow and ice melting could be monitored. Of interest to this study was a series of

14

measurements made when the water was still.

The results of their experiment showed that the convective heat flux (Q_w) was a function of the difference between the bulk water temperature and ice temperature. When this difference was below 3.4 °C, the heat flux increased linearly. Above 3.4 °C, they observed a constant average heat flux of 488.5 W m^{-2} although there was considerable variation due to the variability of the vertical mixing.

Because their study was conducted in an indoor flume, it was not possible to incorporate radiant heating of the water or heat exchange at the water surface. Hence, only the unidirectional transfer of heat stored in the water to the ice surface was involved. More importantly, the effect of wind in forcing convection within the water column and modifying the still water results could not be examined. For these reasons, their laboratory results may be unrealistic under natural conditions.

Wake and Rumer (1979) tried to describe the physical impact a meltwater layer may have on the rate of ice melt in the field. Their one-dimensional, energy balance, ice dissipation model considers three regions: 1) the heat exchange process at the air-ice interface 2) the thermal diffusion of heat through the meltwater layer to the ice-water interface and 3) the absorption of solar radiation at the water-ice interface and ice melt.

According to Wake and Rumer (1979), the presence of a

15

water layer over an ice surface will alter the rate of ice melt from the simpler air-ice (or snow) scenario. They argue that the temperature gradient at the water-ice, rather than the air-water, interface will govern the rate of ice melt. Assuming that the accumulated melt water is stagnant and that the transfer of heat within the water layer is one-dimensional, the mathematical expression governing the temperature distribution in the water column may be expressed as

$$dT/dt = D_w \, d^2T/dz^2 + Q_{in}/ \, \rho_w \, S_w \qquad \text{(Equation 5)}$$

where dT/dt represents the change in water temperature over time ($K \, h^{-1}$), D_w is the vertical thermal diffusivity coefficient which represents the rate at which a thermal disturbance will be transmitted through a substance ($m^2 \, s^{-1}$), d^2T/dz^2, the rate of change of the water temperature gradient ($K \, m^{-2}$), Q_{in}, the heat source per unit volume of water due to absorption of transmitted solar radiation ($W \, m^{-3}$), ρ_w, water density ($kg \, m^{-3}$) and S_w, specific heat of water ($J \, kg^{-1} \, K^{-1}$). The first term on the right-hand side of this equation represents the diffusive heat transport while the second term expresses the internal heating of the water layer due to absorbed radiation. Taking into consideration the physical properties of a water column and an ice surface, Wake and Rumer (1979) expressed Q_{in} as

16

$$Q_{in} = \phi \ K\!\downarrow\!(1-\alpha_w) \ \beta_w \ e^{-\phi z} + \phi \ K\!\downarrow\!(1-\alpha_w) \ \beta_w \ e^{-\phi h} \ \alpha_i \ e^{-\phi(h-z)}$$

<div align="right">(Equation 6)</div>

where ϕ represents the optical extinction coefficient of the water surface (m^{-1}), α_w, water surface albedo (dimensionless), β_w, the fraction of solar radiation transmitted through the water surface (dimensionless), and α_i is the reflectivity coefficient at the water-ice interface (dimensionless).

In order to determine the resultant effect that a meltwater layer has on the rate of basal ice melt, the energy transferred by the physical processes operating at the air-water interface must also be obtained. Wake and Rumer (1979) expressed the energy entering and leaving this interface may be expressed as

$$- \rho_w \ S_w \ D_w \ dT/dz = K\!\downarrow\!(1-\alpha_w)(1-\beta_w) + L\!\downarrow - L\!\uparrow \pm Q_E \pm Q_H$$

<div align="right">(Equation 7)</div>

Incorporating Equations 5 to 7, they were able to theoretically determine the rate of ice melt in an air-water-ice situation. The melt rate at this interface can be mathematically expressed as

17

$$-dh_m/dt = 1/L_f \; \rho_i \; [\rho_w \; S_w \; D_w \; dT/dz$$

$$+ \; K\!\downarrow (1-\alpha_w) \; \beta_w \; e^{-\phi h} \; (1-\alpha_h)(1-\beta_h)\,]$$

(Equation 8)

where the left hand side of this equation represents the rate of ice melt during a time period while the right hand side represents the energy available for ice melt.

Despite the fact that Wake and Rumer (1979) have attempted to mathematically interpret the radiation balance, energy balance and resultant ice melt rate in a air-water-ice network, their analysis is not without fault. In this ice melt model, Wake and Rumer (1979) did not include the possible heat loss into the substrate and they also treated the water as a semi-transparent solid. Their main limitation however, stems from the fact that they were unable to determine the vertical thermal diffusivity coefficient (D_w), which incorporates the thermal effects of convective mixing into Equation 8. To solve this problem, Wake and Rumer (1979) used the molecular thermal diffusivity (the rate at which a thermal disturbance will be transmitted between still particles) of water $(D_m =1.44 \times 10^{-6} \; m^2 \; s^{-1})$ and let it vary through several orders of magnitude to approximate the thermal effects of convection. Although the model was not tested against observed melt data, they simulated melt by employing three diffusivity values (Equation 9 to 11) and several weather

18

scenarios:

$$D_w = D_m \qquad \text{(Equation 9)}$$

$$D_w = D_m \times 10 \qquad \text{(Equation 10)}$$

$$D_w = D_m \times 100 \qquad \text{(Equation 11)}$$

Once the vertical thermal diffusivity values and other appropriate meteorological data were determined, they then proceeded to determine whether the accumulation of water over an ice surface would influence the rate of ice melt.

19

1.2 Objectives

Within the context of the above discussion, the objectives of this study are as follows:

(1) to examine the physical processes and conditions of a supra-ice melt pond,

(2) to determine the vertical thermal diffusivity coefficient. (D_w) of the ponded water,

(3) to investigate the relationship between vertical thermal diffusivity and meteorological variables in order to allow the prediction of thermal diffusivity when detailed pond information is not available.

The first objective will provide basic information for the melt ponds which is currently unavailable in the literature. To model ice melt using the Wake and Rumer (1979) approach, knowledge of the rate that heat moves downward to the ice surface is required. This will be met by the final two objectives.

20

1.3 a Priori Model

The a priori model for this study is given in Figure 1. At the water surface, latent heat flux density (Q_E), sensible heat flux density (Q_H), heat flux due to precipitation (Q_P) as well as terrestrial (L↑) and atmospheric (L↓) long-wave irradiances are exchanged with the atmosphere. The net energy absorbed from the atmosphere enters the water and moves vertically through the water medium via conduction and convection (Q_W). This energy is either stored within the water (ΔQ_S), raising its temperature, or transferred to the ice-water interface where it can be used to melt ice (Q_M). Some of this energy can also be carried downward through the ice by conduction (Q_G) to alter the ice temperature.

Short-wave solar radiation (K↓) also participates in the ice melt process. As K↓ strikes the air-water interface, part of this energy is reflected owing to the albedo of the water surface, while the remainder is transmitted across the interface and into the water column (Viskanta and Toor, 1972; Wake and Rumer, 1979). As the radiation propagates through the water column, some of this radiant energy is absorbed and scattered (Viskanta and Toor, 1972) while the remainder will strike the water-ice interface. A proportion of the radiant energy will reflect owing to the albedo of the ice surface and the remainder will penetrate into the ice and be absorbed.

21
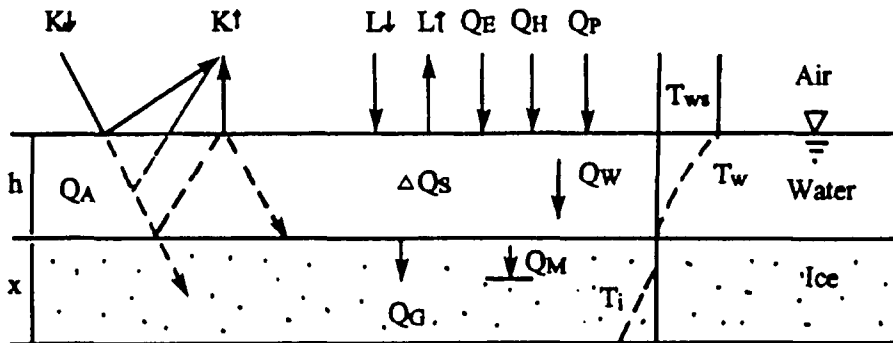
$K\downarrow$ represents incoming short-wave solar radiation; $K\uparrow$, short- wave reflected radiation;

$L\downarrow$, atmospheric long-wave radiation; $L\uparrow$, terrestrial long-wave radiation;

Q_E, latent heat flux; Q_H, sensible heat flux; Q_P, heat flux due to precipitation;

ΔQ_S, storage heat flux; Q_G, heat flux into the ice; Q_W, heat flux in the water due to

conduction and convection; Q_M, melt energy flux; Q_A, absorbed solar radiation;

T_{ws}, water surface temperature; T_w water temperature at depth h; T_i, ice temperature

at depth x.

Figure 1: Energy exchange components for a melting ice surface beneath a layer of water.

22

This absorbed radiation will modify the ice temperature and contribute to ice surface melt (Q_M) and the heat flux through the ice (Q_G). As for the radiant energy which is reflected from the ice-water interface, this will radiate upward until it reaches the air-water interface where some it will enter the atmosphere. The remaining radiant energy will be re-directed toward the ice surface, heating the water column as it is absorbed (Wake and Rumer, 1979).

SITE LOCATION AND INSTRUMENTATION

2.1. Study Site

2.1.1 Location and Climate

This study was conducted during the summer of 1990 on two supra-ice melt ponds located north of Resolute (74° 43'N, 94° 59'W), Cornwallis Island, N.W.T. (Figure 2). Cornwallis Island is situated in the centre of the Canadian Arctic Archipelago and possesses a total land area of approximately 7,382 km^2 (Thorsteinsson and Kerr, 1969). Due to its geographical location, Resolute experiences periods of continuous darkness and daylight during the course of the year. Twenty-four hours of continuous daylight begin during the last days of April and end in mid August. As a result of this diverse radiation regime, Resolute encounters periods of extreme climatic conditions. As shown in Table 1, mean annual temperatures at Resolute Airport for the past thirty years were well below zero. On a monthly basis, mean daily winter temperature conditions have been observed to fall as low as - 35 °C whereas peak summer temperatures generally do not exceed 10 °C. Rainfall occurs only in the summer months, particularly July and August, while snowfall occurs throughout

24
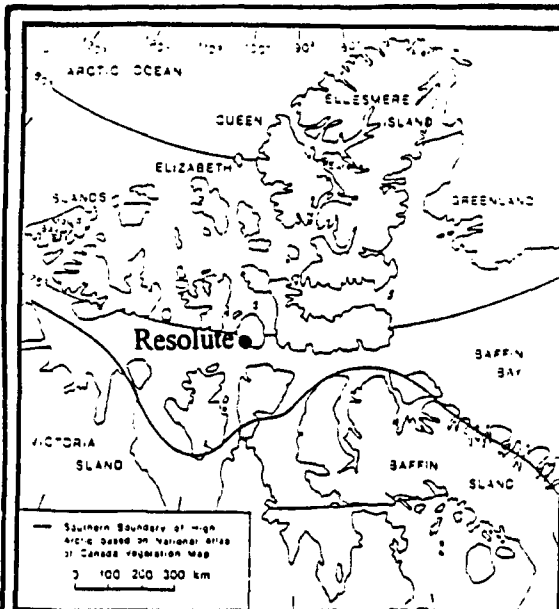
Location of Small Lake ice pond (1)

Location of Channel Pond (2)
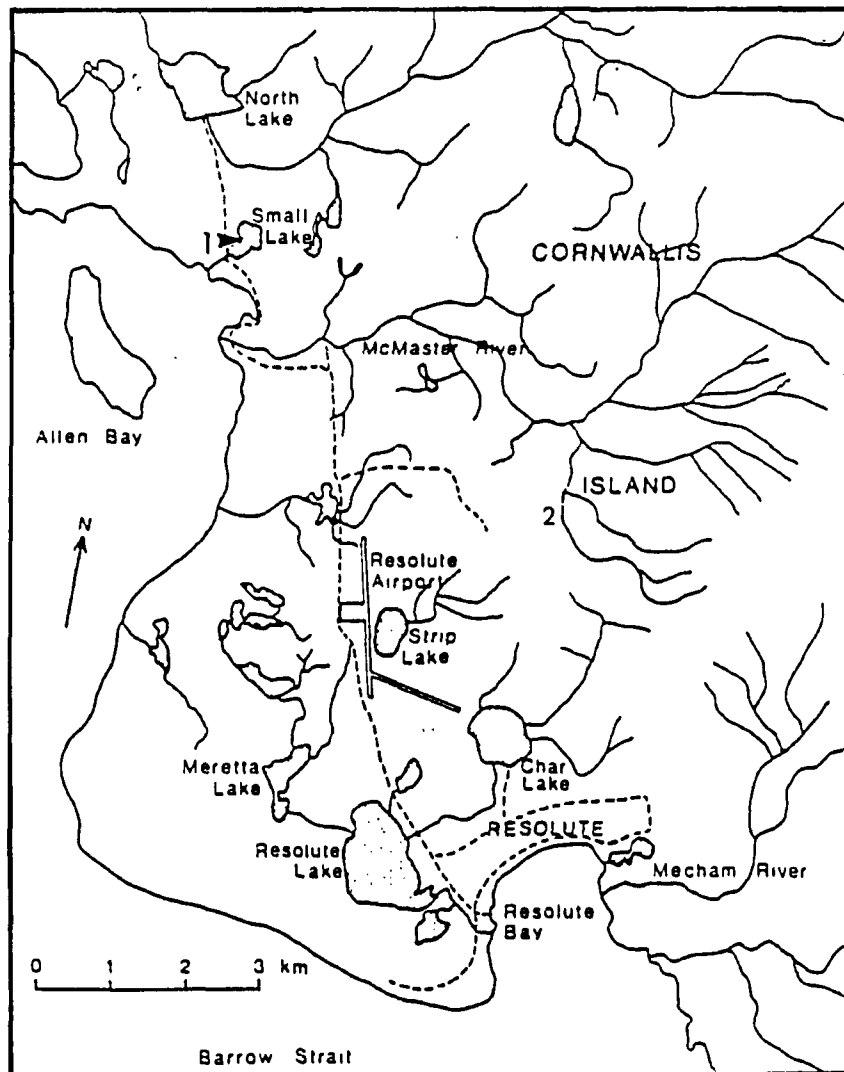
Figure 2: Location of study sites at Resolute on Cornwallis Island
in the Canadian High Arctic.

25

Table 1: Monthly climatic normals for Resolute Airport, N.W.T.

Month	Daily Temp (°C)	Rainfall (mm)	Snowfall (mm)	Days with Rain	Days with Snow
Jan.	-32.1	--	3.4	--	5
Feb.	-33.2	--	3.1	--	5
Mar.	-31.4	--	3.1	--	5
Apr.	-23.1	--	6.5	--	7
May	-10.9	--	9.2	--	9
June	-0.6	5.3	7.0	3	6
July	4.1	19.1	3.3	8	2
Aug.	2.4	24.6	6.7	8	5
Sept.	-5.1	3.7	15.3	1	11
Oct.	-15.1	--	14.8	--	13
Nov.	-24.5	--	6.1	--	7
Dec.	-29.9	--	5.3	--	7

the year and is most prominent during the months of September and October.

2.1.2 Snow and Ice Properties

At the end of the winter season, snow depth near Resolute is highly variable and strongly influenced by local topography. Woo and Marsh (1978) have observed that hill tops usually maintain a low mean snow depth (0.0 - 0.1 m) while topographic depressions such as gullies and valleys possess very high mean snow depths (1.0 - 2.0 m). Average seasonal snow densities near Resolute have been found to remain rather consistent at 310 kg m^{-3} (Bilello, 1969), although an earlier study suggests that snow density may be greater than 350 kg m^{-3} (Williams, 1957).

Studies conducted on sea ice (Bilello, 1980), and lake ice (Heron, 1985) near Resolute Bay show that snow and ice properties are fairly consistent. Snow depth measurements made on the sea ice cover show that mean snow depth may vary from 0.2 m to 0.4 m, while on lake ice, mean snow depth may range from 0.1 m or less to as high as 1.5 m near the edge of the lake. These studies also show that mean sea ice and lake ice thickness may fluctuate between 1.8 m and 2.4 m at winter's end. The average date of maximum ice thickness for lake, sea or river ice in the Canadian Archipelago is June 1, a time when melt may already have started (Bilello, 1980).

27

2.1.3 Supra-Ice Melt Ponds

This experiment was carried out on two shallow, fresh water supra-ice melt ponds. Each melt pond possessed a basal ice layer consisting of white ice. This basal layer was probably created by surface meltwater refreezing to the substrate although in the case of Small Lake, it could have also formed during freeze-up the previous fall.

The ice pond on Small Lake is located near the outlet (Figure 2). The length of this particular pond was 30.0 m with a width of approximately 10.0 m. The white basal ice surface of this supra-ice melt pond was roughly 0.05 m thick and fairly flat with few air bubbles present. At the beginning of this experiment, the pond had a water depth of 0.13 m.

Channel Pond is located approximately 3 kilometres north east of Resolute (Figure 2) and it drained through a wetland area into a tributary of the McMaster River. This supra-ice melt pond was the larger of the two sites studied. The initial length of this ice pond was roughly 70 m with a width of 30 m. Due to the uneven topography of the area, a slush/snow area surrounded the study site. The basal ice surface contained small undulations and had a thickness of approximately 0.25 m. Below this basal ice layer was a clear ice layer of 0.1 m. Unlike the Small Lake ice pond which was located on top of a floating lake ice cover, this supra-ice

28

melt pond was on ice frozen to the bed. The water depth at the beginning of this experiment was 0.075 m.

2.2 Instrumentation and Methods

2.2.1 Apparatus

To obtain appropriate meteorological data for this investigation, all field instruments were suspended above each supra-ice melt pond (Figure 3). The instruments were clamped to a 2.5 meter long metal bar which was supported by a camera tripod at each end. Due to water level changes, the instruments were between 0.25 m and 0.55 m above the surface of the water. Data from each instrument were gathered every minute and averaged for one-half hour, using a Campbell Scientific CR21 data logger.

2.2.2 Meteorological Measurements

Two Kipp and Zonen (CM-5) hemispherical radiometers measured the amount of incident ($K\downarrow$) and reflected ($K\uparrow$) short-wave solar radiation striking and leaving each supra-ice melt pond. A Frichen type radiometer was used to determine the net radiation of the supra-ice melt pond. Wind speed was measured with a small R.M. Young cup anemometer. A Campbell Scientific thermistor (Model 101) was used to record air temperature and a Campbell relative humidity sensor (Model 201) measured relative humidity. To avoid the absorption of
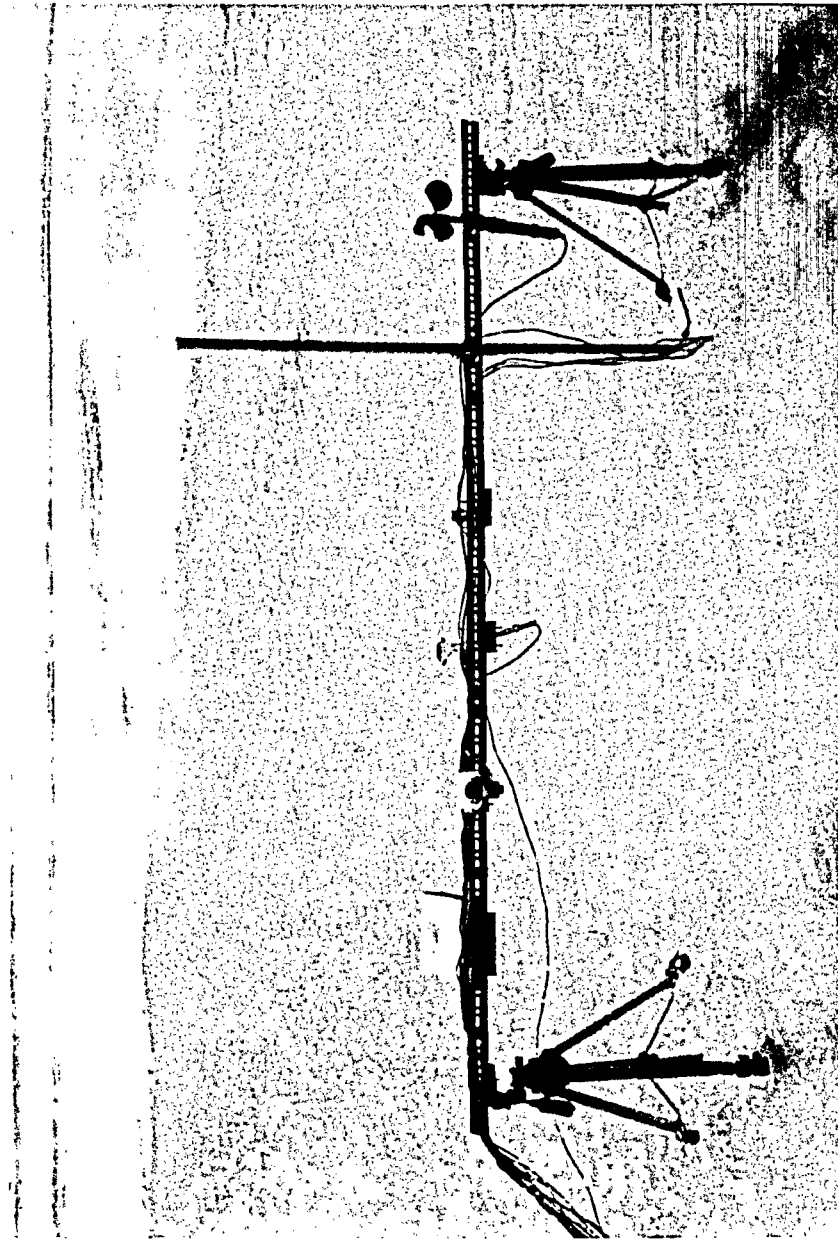
29

Figure 3:   Photograph of the instrumentation installation and melt pond conditions at Small Lake.

30

solar radiation, the thermistor and relative humidity sensor were placed in a white, wooden, naturally ventilated shield.

2.2.3   Water Temperature

Four or five thermistors (Fenwell #JB32P2) were used to determine pond water temperature. The thermistors and their supporting plexiglass extensions were painted white to avoid solar radiation absorption. A vertical white wooden support attached to the horizontal bar held the thermistors at their assigned distances of 0.005 m, 0.20 m, 0.40 m, and 0.60 m above the ice surface. The vertical support could be adjusted to account for ice melting when necessary. In order to determine water surface temperature, an identical thermistor (Fenwell #JB32P2) was attached to the underside of a small piece of styrofoam allowing it to remain at the water surface.

2.2.4   Ice Melt

For this investigation, ice melt measurements were obtained along two transects. The plexiglass tubes (0.02 m in diameter and snowfilled when possible) were manually inserted into holes drilled up to 0.3 m into the ice. They were spaced approximately 1 m apart. Thin string, with its ends tied to each plexiglass rod was stretched tightly above the pond surface to act as a reference datum. Approximately 10 points were located on the string and the distance between the ice

31

surface and the clearly labelled string enabled the amount of
ice melt between observations to be measured.

2.2.5 Water Level

For each supra-ice melt pond, water depth was also
determined using the reference datum described above. Water
depth measurements were obtained below each reference point
using a metal ruler. Due to the unevenness of each basal ice
surface, the results were averaged.

2.2.6 Energy Exchange

2.2.6.1 Net Long-Wave Flux

While incoming (K↓) and outgoing (K↑) short-wave solar
radiation and net radiative flux (Q*) were measured directly
above the supra-ice melt pond, atmospheric (L↓) and
terrestrial (L↑) long-wave radiation were determined in a
different manner. L↑ was determined indirectly using the
Stephan-Boltzman Law:

$$L\uparrow = e\ \tau\ T_{ws}^{4} \qquad\qquad \text{(Equation 12)}$$

where e represents the emissivity of the water surface (0.97),
τ, the Stephan-Boltzman constant ($5.67 \times 10^{-8}\ Wm^{-2}\ K^{-4}$) and T_{ws},
is the water surface temperature (K).

After having determined L↑ for each desired time
interval, L↓ was calculated by rearranging the net radiation

32

balance equation (Equation 2) to

$$L\downarrow = Q* - K\downarrow + K\uparrow + L\uparrow \qquad \text{(Equation 13)}$$

Once atmospheric and terrestrial long-wave radiation were computed, the net long-wave flux ($L*$) absorbed or released from the melt pond surface was determined by

$$L* = L\downarrow - L\uparrow \qquad \text{(Equation 14)}$$

2.2.6.2 Sensible and Latent Heat Exchange

The fluxes of sensible (Q_H) and latent heat (Q_E) were obtained using the aerodynamic bulk exchange method. This approach is very practical as it does not require extreme measurement precision, thus permitting robust equipment to be employed (Munro, 1990). It offers advantages over empirical functions incorporating wind since it accounts for the effects of the surface, atmospheric stability as well as measurement height and does not require calibration for each site. The sensible and latent heat fluxes are

$$Q_H = \rho_a \, S_a \, D_H \, U_a \, (T_a - T_{ws}) \qquad \text{(Equation 15)}$$

$$Q_E = \rho_a \, L_v \, (\varepsilon/P) \, D_E \, U_a \, (e_a - e_{ws}) \qquad \text{(Equation 16)}$$

where S_a refers to the specific heat of air ($J \ kg^{-1} \ K^{-1}$), L_v is

33

the latent heat of vaporization ($J\ kg^{-1}$), ε is the ratio of the molecular weights of water and air (dimensionless), P is the atmospheric pressure (Pa), D_H and D_E are dimensionless exchange coefficients and e_{ws} and e_a are the vapour pressure (Pa) at the water surface and at a height of z meters above the water surface, respectively.

The exchange coefficients (D_H, D_E) were assumed to be equal and were obtained from

$$D_H = D_E = D = k^2\ /\ [\ln\ (z_a/z_o)]^2 \qquad \text{(Equation 17)}$$

where k, is the dimensionless von Kármán constant (0.4), z_a, the height above surface (m) and z_o, surface roughness parameter (m). In the event of stable or unstable atmospheric conditions, the exchange coefficient (D) was altered using the Richardson number, R_i, as described by Price et al. (1976).

$$R_i = gz\ (T_a - T_{ws})\ /\ T_a\ (U_a - U_s)^2 \qquad \text{(Equation 18)}$$

where U_a refers to wind speed at height z_a (m s^{-1}) and U_s the surface wind speed (m s^{-1}). For stable atmospheric conditions ($R_i > 0$), the exchange coefficient (D_s) was adjusted to

$$D_s = D\ /\ (1 + \delta R_i) \qquad \text{(Equation 19)}$$

where δ is a dimensionless coefficient assigned a value of 10.

34

When unstable (D_u) atmospheric conditions prevailed, ($R_i < 0$), the drag coefficient was modified using

$$D_u = D (1 - \delta R_i) \qquad \text{(Equation 20)}$$

To employ these equations, air temperature and humidity were measured between 0.25 and 0.45 m above the pond surface as a result of variations in the water level. The water level was measured at each visit and linearly interpolated to allow estimation of the instrument height (z) between visits. The vapour pressure of the water surface (e_w) was derived from direct water temperature data. The numerical estimates of the atmospheric vapour pressure (e_a) were determined from relative humidity measurements as outlined by Dilley (1968).

To provide an unobstructed flow of air, the cup anemometer was positioned approximately 0.15 m above all other instruments. Assuming a logarithmic wind profile above the supra-ice melt pond, wind speed was adjusted to account for the additional height using

$$U_a = U_m (\log(z_o) - \log (z_a)) / (\log(z_o) - \log(z_m))$$

$$\text{(Equation 21)}$$

where U_m is the wind speed (m s^{-1}) measured at height z_m and z_a is the height at which wind speed (U_a) is to be estimated. The surface roughness parameter (z_o) is controlled by the

35

water surface and for this study was assigned a value of 0.002 m (Oke, 1987).

The assumptions underlying the formulation of the aerodynamic bulk transfer method have been discussed by Moore (1983) and Hay and Fitzharris (1988). The most important one with respect to this study is the measurement of the atmospheric variables within the internal boundary layer in which the turbulent fluxes are constant with height and the temperature, humidity and wind profiles are log-linear. When the fetch is limited, this layer may be thinner than the measurement height. To ensure that the boundary layer is sufficiently developed, the conventional rule-of-thumb is to allow 100 m of fetch for each meter of boundary layer height (Male and Granger, 1981). This may be a conservative estimate as indicated by Andreas (1982), one of the few studies to examine boundary layer development. Using atmospheric data dealing with the transition from sea ice to leads, and pavement to grass, Andreas (1982) found that the boundary layer thickness increased very rapidly, reaching 0.6 m with 2 to 3 m of fetch and 1 m after a fetch of about 6 m. If this is a reasonable approximation of the behaviour to be expected at the melt pond sites, then with few exceptions, the measurements of air temperature, humidity and wind speed should be within the boundary layer. The profiles may vary from the ideal log-linear form in calm conditions, but the fluxes of latent and sensible heat will be small under these

36

conditions.

There has been some discussion in the literature about the validity of the other two main assumptions of equality of the exchange coefficients and equality of the scaling (or roughness) lengths and how they should be dealt with. Few studies have examined the validity of these assumptions in non-ideal field conditions and there is no estimate of the errors produced when the assumptions are violated (Moore, 1983).

2.2.6.3 Absorbed Solar Radiation

Short-wave radiation is absorbed by the water column and used to raise its temperature. The greatest absorption occurs as the radiation penetrates downward from the water surface while a much smaller amount is absorbed from radiation reflected from the water-ice interface.

Based on Beer's Law, Wake and Rumer (1979) give the radiation flux reaching the ice-water interface (F_i) as

$$F_i = (1-\alpha_w) \ \beta_w \ K\!\downarrow \ e^{-\phi h}$$ (Equation 22)

The radiant energy absorbed in the first pass through the water (Q_{A1}) is then

$$Q_{A1} = (1-\alpha_w) \ K\!\downarrow \ - \ F_i$$ (Equation 23)

37

For this investigation, the albedo of the water surface (α_w) was determined using

$$\alpha_w = 0.108 - 0.000139 \text{ K}\downarrow \qquad\qquad \text{(Equation 24)}$$

This linear regression equation was selected from amongst other equations because it implicitly incorporates the influence of solar zenith angle and cloud cover on albedo (Henderson-Sellers, 1986). While Equation 24 is fairly accurate in predicting the albedo of the water surface when incoming short-wave radiation totals fall within 0.0 to 400.0 W m^{-2}, it was frequently observed that this range was exceeded near midday. To solve this problem, the albedo of the ice surface was fixed at a constant value of 0.053 when the short-wave radiation exceeded the upper value.

Within the scientific literature, it is well documented that the absorption of incoming short-wave solar radiation by water is largely a function of wavelength and transparency of the water medium (Drake and Harleman, 1969; Viskanta and Toor, 1972; Pivovarov, 1972). Since the use of a bulk extinction coefficient will underestimate the rapid absorption of the longer wavelengths near the water surface, Wake and Rumer (1979) assumed that 60 % of the total incoming short-wave solar radiation would be absorbed within a very small depth beneath the water surface. Hence B_w, the fraction of solar radiation transmitted through the water surface, was set to

38

0.4. Given the clarity and relative depth of the meltwater accumulated, an extinction coefficient of 0.3 m^{-1} was selected for this analysis (Wetzel, 1975).

Of the radiation reaching the ice-water interface, some will penetrate into the ice while the remainder will be reflected by the interface back towards the water surface. The albedo of the water-ice interface (α_i) was computed by re-arranging the reflectance equation for a two-layered system as described by Boslenga (1981)

$$\alpha_i = (e^{-\phi h}) \, (K\uparrow/K\downarrow - \alpha_w) \, (1 - \alpha_w) \qquad \text{(Equation 25)}$$

The amount of radiation absorbed following reflection by the water-ice interface (Q_{A2}) was computed from

$$Q_{A2} = F_i \, (1 - e^{-\phi h}) \qquad \text{(Equation 26)}$$

By adding Equations 23 and 26, the total radiant energy absorbed directly and indirectly in the supra-ice melt pond can be determined.

$$Q_A = Q_{A1} + Q_{A2} \qquad \text{(Equation 27)}$$

Although more radiation is absorbed following additional secondary reflections, the amount is not significant.

39

2.2.6.4 Storage Heat Flux

Any imbalances between the incoming and outgoing heat fluxes will alter the amount of heat stored by the ponded water. The change in heat storage (ΔQ_s) (W m^{-2}) of the entire pond was obtained by summing the heat gained in the water from the thermistors using

$$\Delta Q_s = \sum_{n=1}^{5} (T_{n\,(t)} - T_{n\,(t-1)})\ h_n\ C_w \qquad \text{(Equation 28)}$$

where h_n is the layer thickness (m) and T_n is the temperature (K) of the water layer (n) at time (t) and (t-1).

2.2.6.5 Energy Flux Used to Melt Basal Ice

The energy flux used to melt the ice surface at the base of the supra-ice melt pond (Q_M, W m^{-2}) was computed using manual ice lowering measurements made in the field:

$$Q_M = -h_m/\Delta t\ L_f\ \rho_i \qquad \text{(Equation 29)}$$

where $-h_m/\Delta t$ is the rate of ice loss (m s^{-1}) and L_f represents the latent heat of fusion (kg m^{-3}).

2.2.6.6 Heat Flux into the Ice

While much of the energy being transferred downward through the water column is used to melt ice, some of it may

40

be conducted downward through the ice to warm the ice or the soil substrate. The ground heat flux can be calculated using

$$Q_G = -k_i \, \Delta T \, / \, \Delta Z \qquad \text{(Equation 30)}$$

where k_i is the thermal conductivity of the ice medium (W m^{-1} K^{-1}) and $\Delta T \, / \, \Delta Z$ is the temperature gradient (K m^{-1}) (Male and Gray, 1981). Temperature profiles are difficult to obtain in the field as radiation frequently melts out wires and thermistors that are placed in the ice. Due to such difficulties, Q_G was examined by simulating the thermal conditions that might be expected in the ice given the observed environmental conditions.

The thermal behaviour of a material absorbing radiation can be described by Equation 5, where the terms on the right hand side account for the diffusion of heat by conduction and the internal heating caused by the absorption of radiation. Since Equation 5 does not have an analytical solution for the general case, the temperature profile in the ice substrate was simulated using the explicit numerical scheme outlined by Fertuck et al. (1971).

$$T_{m,\,n+1} = (T_{m-1,n} + (M-2) \, T_{m,n} + T_{m+1,n}) / M \qquad \text{(Equation 31)}$$

$$M = \rho_i \, S_i \, \Delta x^2 \, / \, k_i \, \Delta t \qquad \text{(Equation 32)}$$

Here, m refers to depth nodes Δx apart at which temperature

41

($T_{m,n}$) will be calculated. The adjacent nodes are m+1 (below) and m-1 (above). The time interval between the current time (n) and next time (n+1) is expressed as Δt. To assure the accuracy of this approach two requirements need to be satisfied: 1) a minimum of six distance increments in the ice medium and 2) a minimum M value of 2. For this investigation, twenty-one distance increments were established for an initial temperature profile. To maintain a minimum M value of 2, a time step increment (Δt) of 7.5 minutes and a node spacing (Δx) of 0.03322 m were used to simulate new temperature profiles within the ice cover.

The radiation absorbed within an ice layer was obtained by

$$Q_I = (1 - \alpha_i) \cdot F_i \left(e^{\phi h i} - e^{\phi(h i - \Delta x)}\right)$$ (Equation 33)

where hi is the distance from the ice-water interface (m). The absorbed radiation flux was converted to a temperature increase (ΔT_R):

$$\Delta T_R = Q_R \Delta t / C_i \Delta x$$ (Equation 34)

and added to the temperature of each corresponding node prior to the next iteration of Equation 33.

To make this procedure operational, the observations of Marsh (1984) and Heron (1985) were used to establish an

42

initial linear temperature profile with gradient of 16.36 °C m^{-1}. The extinction coefficient of the ice was set to 4.0 m^{-1} (Williams, 1971) and thermal conductivity of the ice was 2.24 W m^{-1} K^{-1} (Oke, 1987). The observed temperature and radiation data were interpolated into 7.5 minute intervals and the ice-water interface was lowered at the rate measured in the field. The temperature profiles were reported half-hourly along with the predicted heat flux due to conduction (Q_G).

2.2.7 Vertical Thermal Diffusivity

The Wake and Rumer (1979) one-dimensional ice dissipation model (Equations 5 to 8) required vertical thermal diffusivity for the water in order to predict ice melt. Initially, it had been planned to use the original Wake and Rumer (1979) program code along with field observations to estimate the necessary thermal diffusivity values. Unfortunately, this computer program is no longer available and reconstructing it was beyond the scope of this thesis. Nevertheless, it is still possible to estimate values from the field data.

In Equation 8, Wake and Rumer (1979) assigned ß$_h$ a value of 0.8, assuming that like the water surface, the ice surface would absorb 20 % of the radiation available to be transmitted through it. However, all of the energy in the easily absorbed longer wavelengths are lost at the water surface with blue wavelengths having most of the remaining energy. Since these also easily penetrate ice, it is unlikely that much radiant

43

energy, above that specified by Beer's Law with a constant bulk extinction coefficient, would be absorbed at the surface. Thus, absorbed short-wave radiation will not contribute to melt at the ice surface but may instead alter the heat flux into the ice (Q_G) and reduce the density of the ice through internal melting.

As a result, the energy balance at the ice-water interface will be

$$Q_W = Q_M + Q_G \qquad \text{(Equation 35)}$$

The energy to produce ice melt is being provided by the heat flux from the water (Q_W) and consumed by ice melt (Q_M) and the heat flux into the ice and substrate (Q_G). The water heat flux density (Q_W) can be determined from

$$Q_W = C_w \, D_g \, (\Delta T / \Delta z) \qquad \text{(Equation 36)}$$

where $\Delta T / \Delta z$ is the temperature gradient in the water layer adjacent to the ice cover. Since Q_M can be determined from Equation 29 and Q_G estimated from the finite difference model (Equation 31), the thermal diffusivity can be estimated by equating Equations 35 and 36. Depending on which water temperature and depth observations are used to approximate the temperature gradient, two different thermal diffusivities can be obtained. Using the water surface temperature and pond

44

depth, the thermal diffusivity of Wake and Rumer (1979) (D_w) will result. It will be called the effective thermal diffusivity since it will incorporate the effects of pond depth and convection. The thermal diffusivity just above the ice water interface (hereafter called interfacial thermal diffusivity) can be calculated by using the water temperature measured at 0.005 m above the ice interface to estimate the temperature gradients.

CHAPTER 3

OBSERVATIONS AND RESULTS

3.1.0 Meteorological Conditions

3.1.1 Radiation (K↓, K↑, Q*)

The meteorological variables measured above the Small Lake ice pond are shown in Figure 4. Incoming short-wave solar radiation (K↓), reflected radiation (K↑), and net all-wave radiation (Q*) all followed a regular daily pattern. Low values of radiation were observed in the early morning and late evening hours, while high radiation fluxes occurred near midday. The data also show that positive radiation occurs at night due to 24 hours of sunlight experienced during this time period. Cloud cover produced low K↓, K↑, and Q* values on June 21st while higher totals were observed during June 20th and 22nd with clearer skies.

Figure 5 represents meteorological observations over Channel Pond. The radiation displayed the same daily fluctuating pattern as noted above but there was little variation between days. Incoming short-wave solar radiation (K↓) peaked near 800 W m^{-2}, while reflected short-wave solar radiation (K↑) and net all-wave radiation (Q*) were less than 250 W m^{-2} and 450 W m^{-2}, respectively.
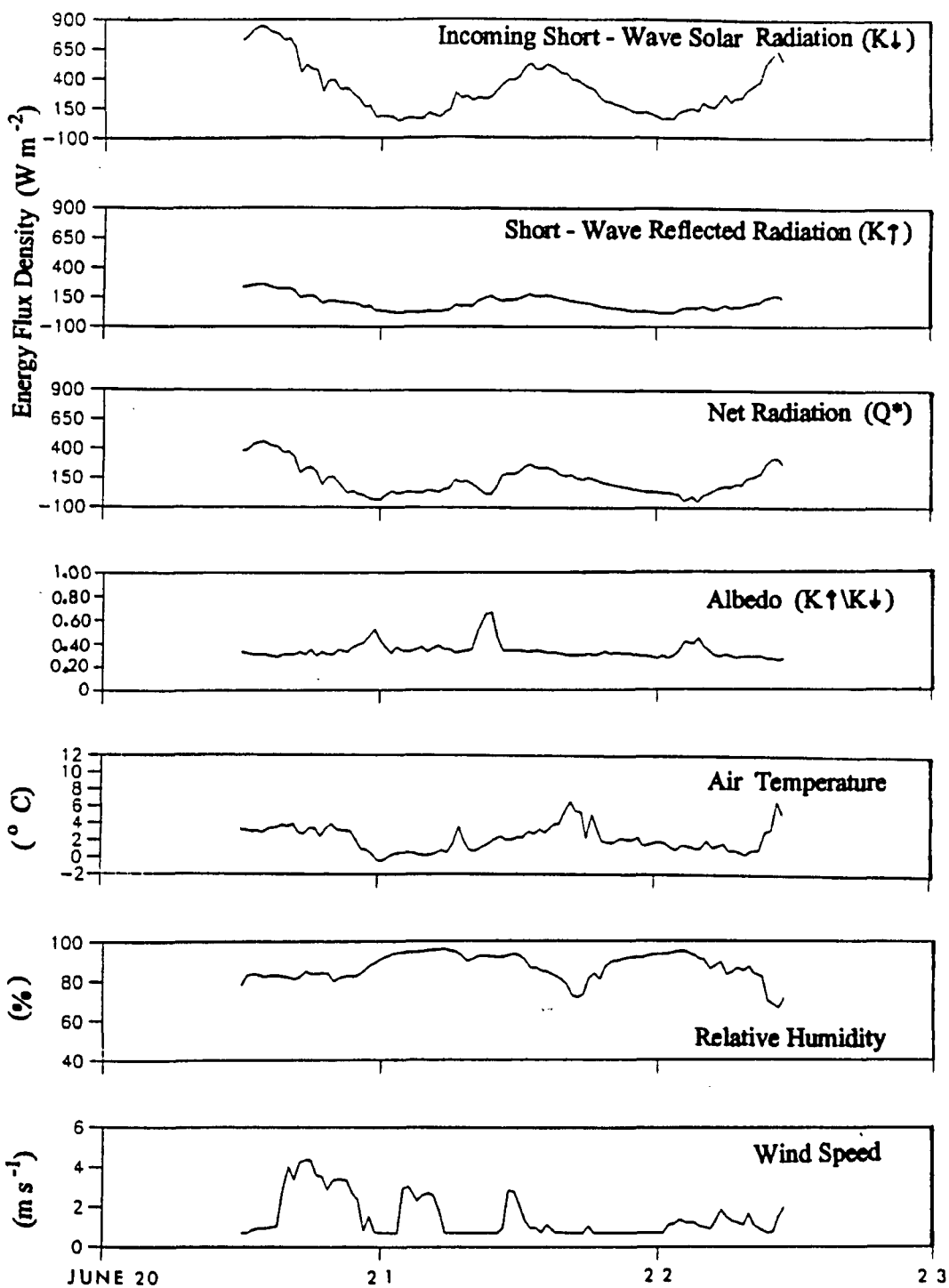
46

Figure 4: Meteorological observations above the water surface of the Small Lake ice pond.
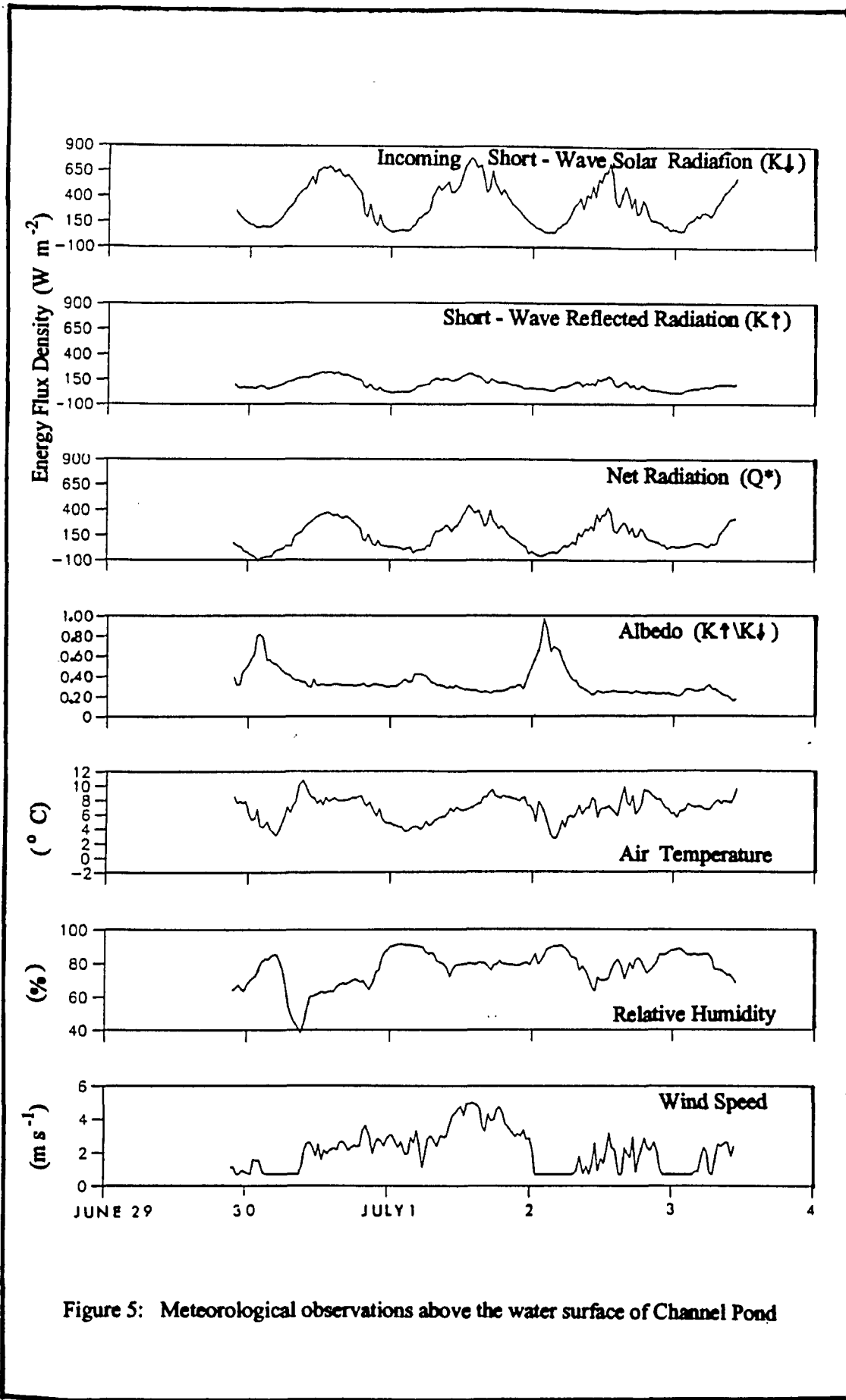
47

Figure 5: Meteorological observations above the water surface of Channel Pond

48

3.1.2 Albedo

Albedo is the ratio between the total amount of incoming short-wave solar radiation falling upon a surface and the amount reflected back into the atmosphere and is usually expressed as a decimal fraction or percentage. Any variation in albedo is largely a function of surface texture, colour as well as the angle at which the sun's rays strike the earth.

The total albedo data obtained above the Small Lake ice pond displayed a rather irregular daily cycle. While high albedo values should occur in the early morning and late evening due to the low elevation of the sun above the horizon, Figure 4 shows that maximum albedo values were observed near midday of June 21st. Although present, this extraneous value was probably due to difficulties in keeping the radiometers level. Otherwise, the remaining albedo values for the Small Lake site appear to follow the expected pattern.

The temporal pattern of total albedo for Channel Pond displayed a less than perfect daily pattern (Figure 5). On June 30th and July 2nd, the albedo of this particular ice pond approached unity. While this may have been the direct result of wind induced ripples and/or levelling difficulties experienced in the field, the rather large blocks of floating ice observed in the early morning hours of July 2nd may have also contributed. Overall, the data show that the total albedo of this ice pond steadily decreased from an average

49

value of 0.35 to approximately 0.20 over the four day period. These results are consistent with the observations of Langleben (1968; 1972) who obtained a value of 0.3 for the albedo of ponds on melting sea ice.

3.1.3 Air Temperature

Air temperature values above each supra-ice melt pond were observed to vary strongly throughout the day. Nonetheless, a daily cycle existed at each site. Low air temperatures were observed in the early morning and late evening hours while high air temperatures occurred near midday or early afternoon.

The greatest air temperature recorded above the Small Lake ice pond was 6 °C on June 21st, despite low incoming short-wave solar radiation. Air temperature fell below 0 °C only briefly on one occasion.

The air above Channel Pond was warmer with numerous temperatures above 8 °C (Figure 5). Air temperatures did not drop below 2 °C. At this time, most of the surrounding terrain was snow-free and warm air was being advected over the site.

3.1.4 Relative Humidity

Relative humidity is the ratio of the air's water vapour content to its water vapour capacity expressed as a percentage. Since it is strongly influenced by air

temperature, a daily cycle was observed at both sites (Figures 4 and 5). Peak relative humidity values in the early morning or late evening rarely exceeded 95 %. During the warmest days, relative humidity could decrease to 50 %, or less.

3.1.5 Wind Speed

Anemometer readings obtained above each ice pond (Figure 4 and 5) indicate that wind speed fluctuated considerably throughout the day. There were also frequent calm periods. These periods appear in Figures 4 and 5 as non-zero values since the anemometer has a stalling speed of 0.7 m s^{-1}. While wind speed typically fell within the 2.0 m s^{-1} to 3.0 m s^{-1} range, maximum speeds near 5.0 m s^{-1} were observed at Channel Pond.

3.2 Pond Conditions

3.2.1 Water Temperature

Water temperatures recorded at different levels in the Small Lake ice pond and Channel Pond are illustrated in Figures 6 and 7. The data show that a regular diurnal temperature pattern was established at each location. In general, low water temperatures were observed in the early morning and late evening hours while high water temperatures were recorded shortly after midday.

In comparing water temperature data recorded at different levels, each display shows that water temperatures closely
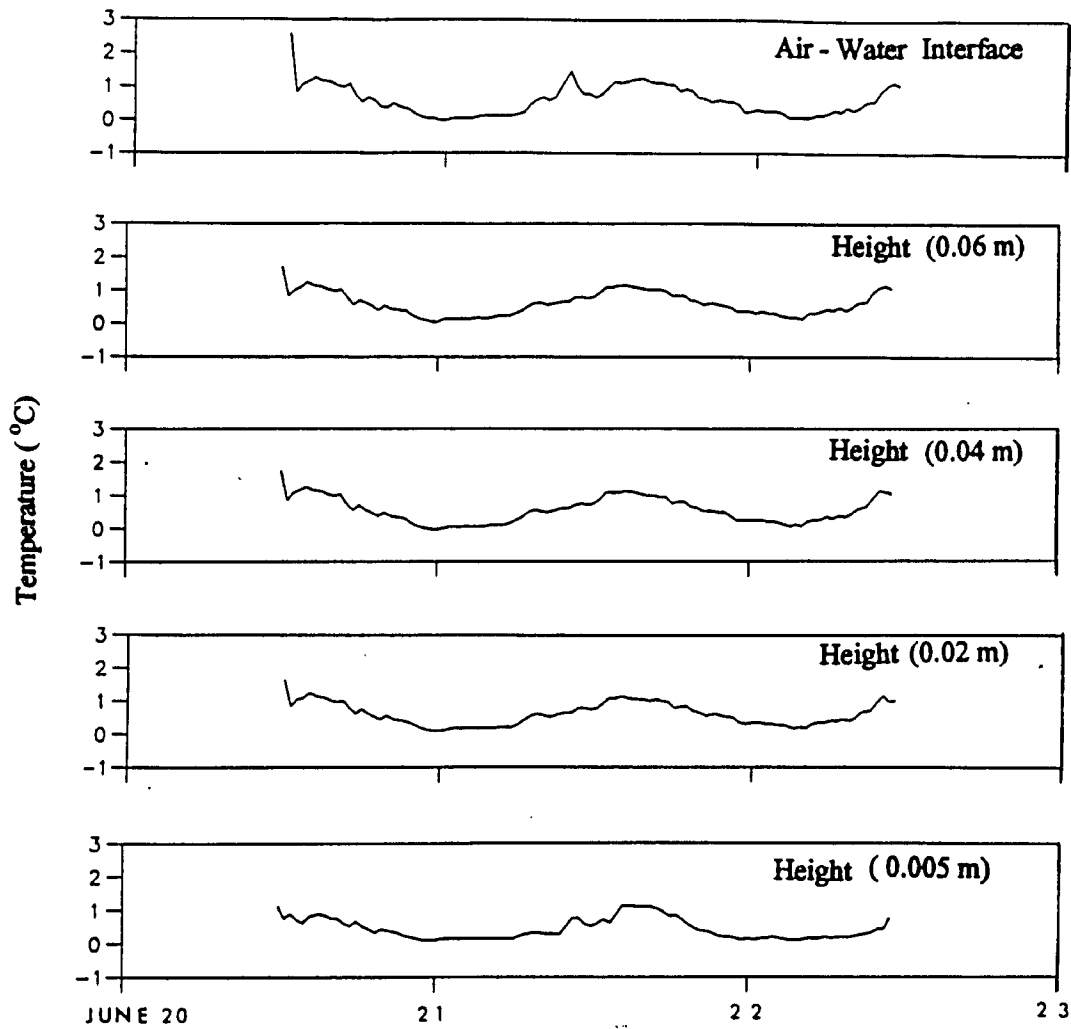
51

Figure 6: Water temperatures recorded at different depths within the Small Lake melt pond.
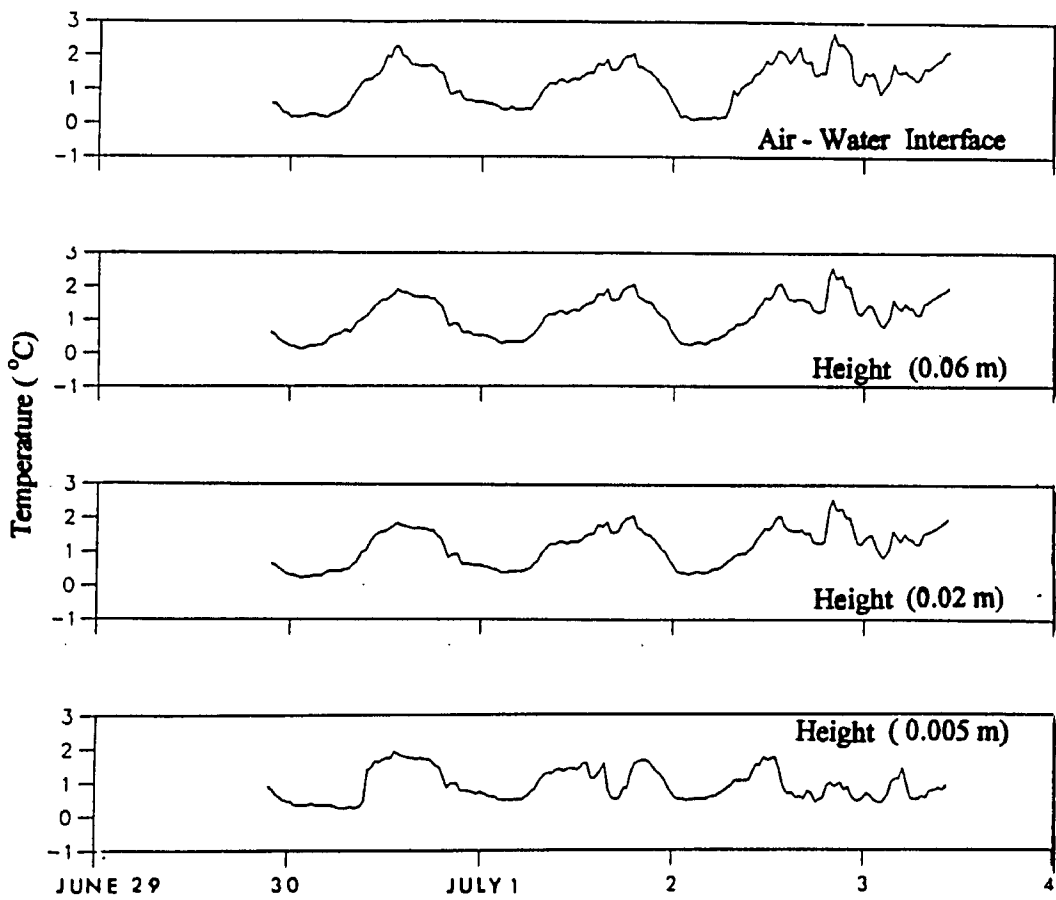
52

Figure 7: Water temperatures recorded at different depths within Channel Pond.

53

resemble one another. It must be noted however that some deviations at the surface and bottom thermistors are present. The data also show that ice pond water temperatures never fall to 0 °C and typically range between 0.1 °C and 3.0 °C. A comparison of the two sites studied show that Channel Pond possessed the higher temperature readings. This difference was primarily the result of greater radiation and air temperatures experienced during this period (Figures 4 and 5).

The profiles indicate that most of the water column is at approximately the same temperature. The systematic deviations from a smooth profile especially evident in the Small Lake data can be attributed to calibration and measurement errors. The accuracy of the temperature measurements is approximately 0.1 °C.

Just above the ice-water interface is a layer of water in which the temperature gradient is very steep as the temperature decreases from that in the convective layer. In the Small Lake site, this transition was more gradual than in Channel Pond.

The diurnal pattern of warming and cooling described above is also evident in Figure 8. While the bulk of the water column tends to warm and cool relatively evenly, there is a subtle change in the temperature gradient in the convecting layer. In the morning when heating is rapid, the
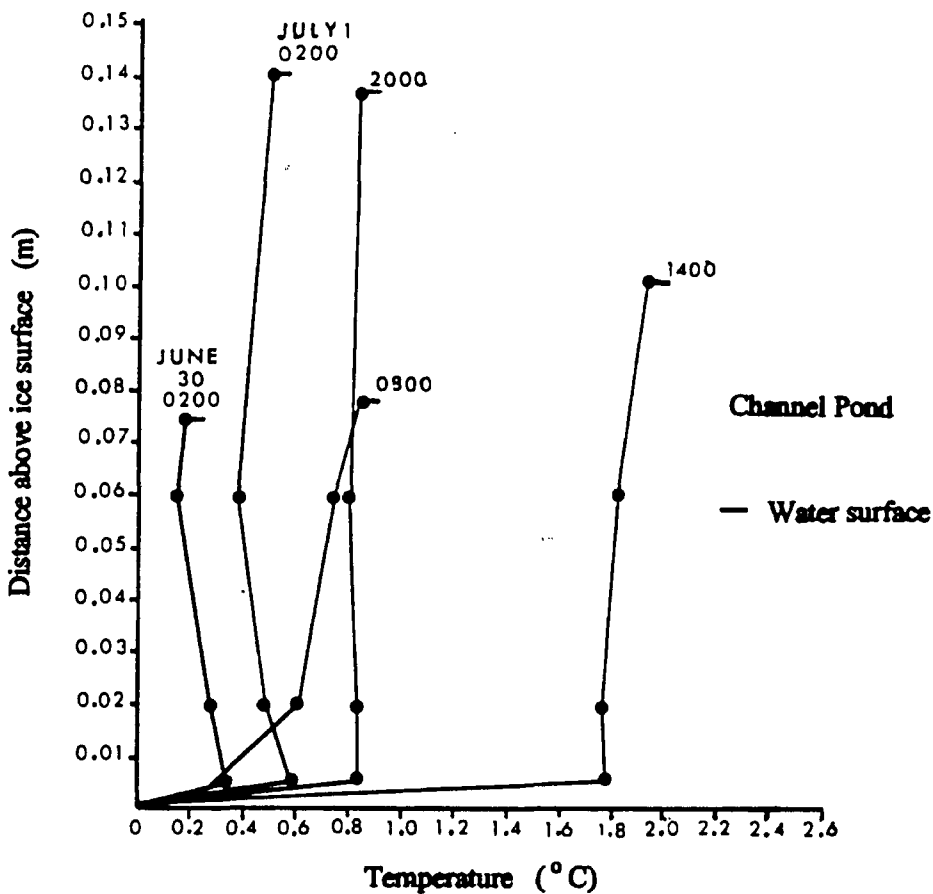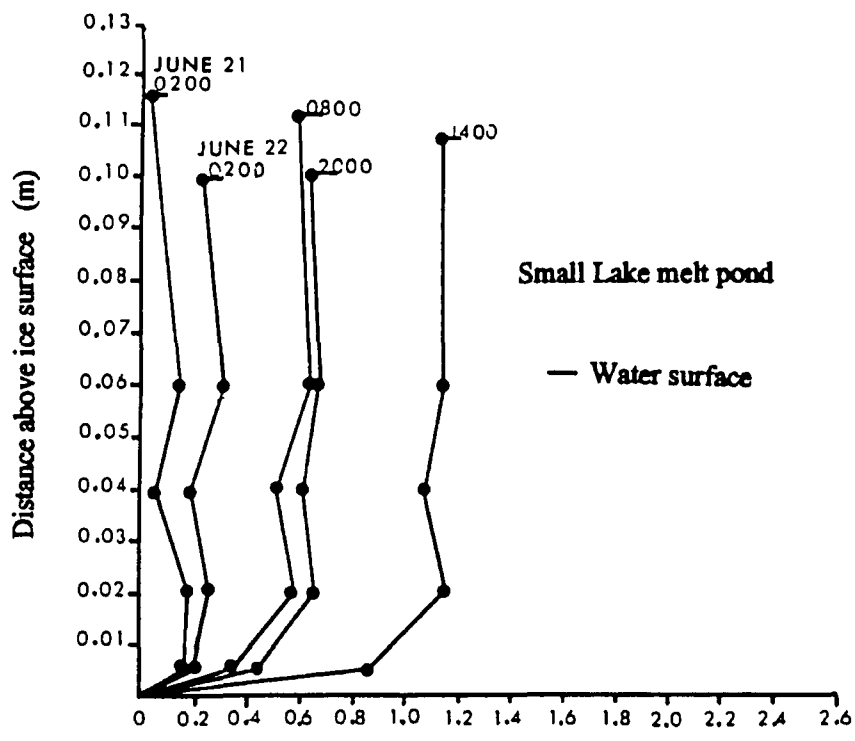
54

Figure 8: Selected water temperature profiles on June 21st from the Small Lake melt pond and June 30th from Channel Pond.

55

water surface tends to be warmer and the temperature decreases slightly with distance below the surface. During the evening and night, the loss of energy from the water surface cools the surface water and the warmest water may be found just above the ice surface. These temperature gradient differences are not always present and will depend upon the rate of mixing within the convection layer.

3.2.2 Ice Melt

Ice melt measurements made on the Small Lake ice pond are found in Figure 9. In general, the ice melt rate followed a daily pattern (Figure 9a) and was strongly influenced by water temperature (Figure 6). When water temperatures are cold, such as in the early morning and or late evening, ice melt rates are low (Figure 9b). As the overall temperature of the supra-ice melt pond increased, so to did the rate of ice melt. Ice melt on the Small Lake ice pond varied from 0.5 mm h^{-1} to as high as 2.0 mm h^{-1}.

Ice melt measurements made at two different locations in Channel Pond are illustrated in Figure 10. A comparison of the data reveals that ice melt was quite consistent throughout, despite the primitive means by which ice melt was determined. As in the previous example, ice melt rates were observed to be strongly influenced by water temperature (Figure 8) and appear to follow a daily cycle (Figure 11). The rates of ice melt in Channel Pond however, were observed

56

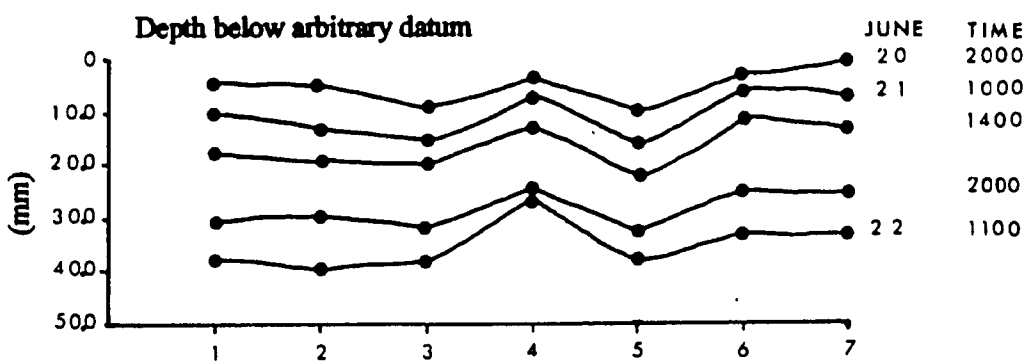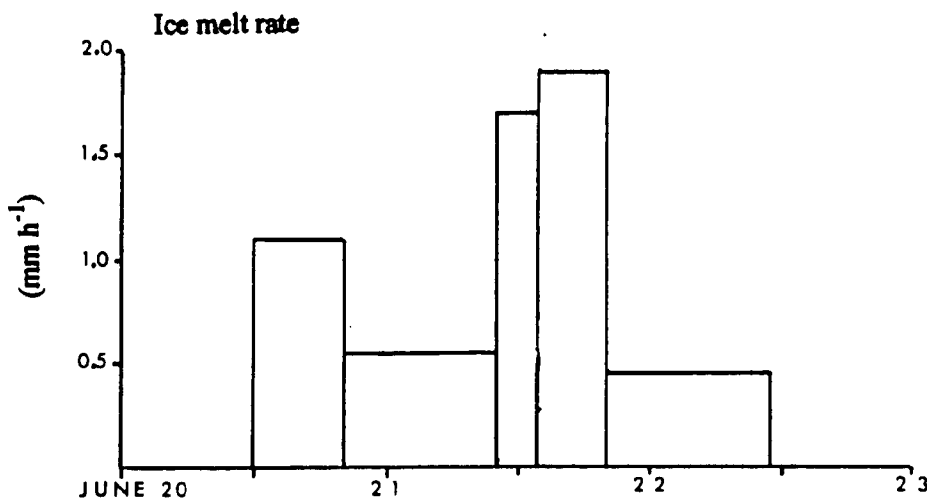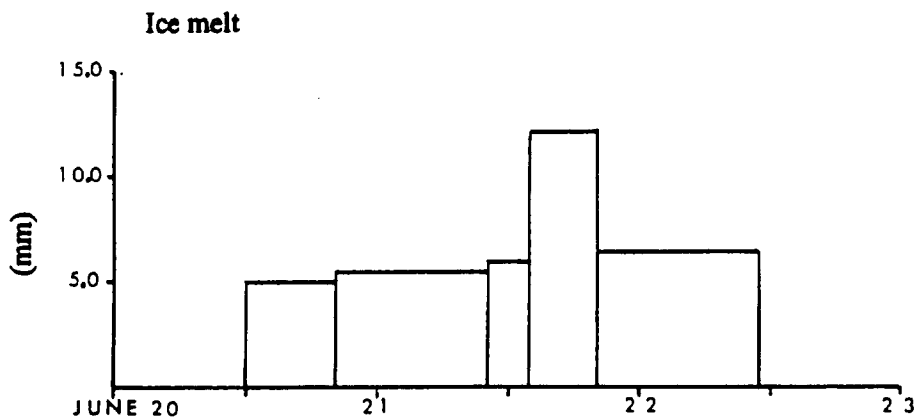Ice melt

Ice melt rate

Depth below arbitrary datum

Figure 9: Ice melt measurements for Small Lake melt ponds(a) depth of ice melt, (b) ice melt rates, (c) cross sections of the basal ice surface throughout the study period.
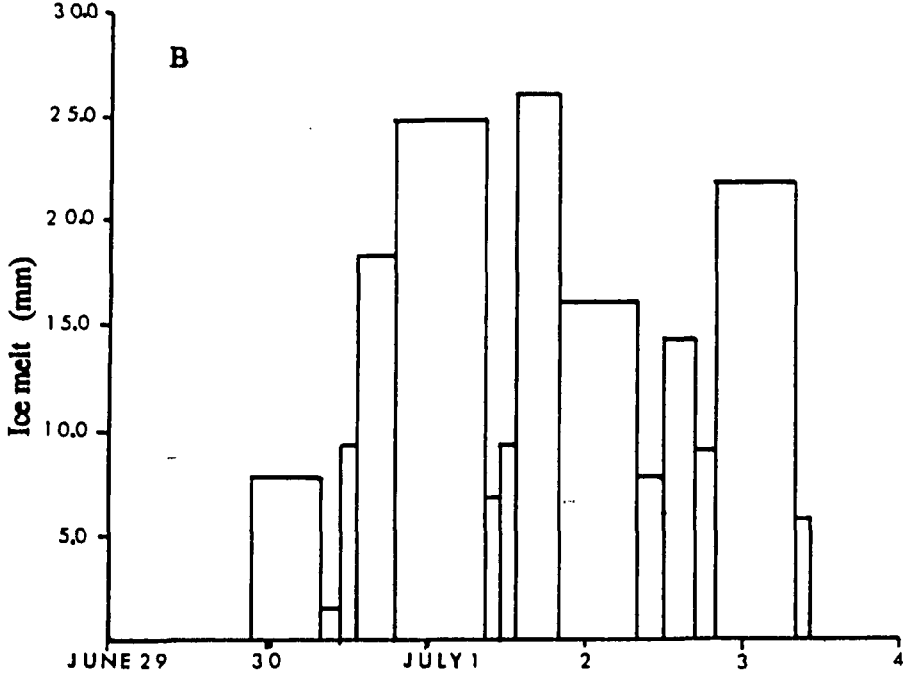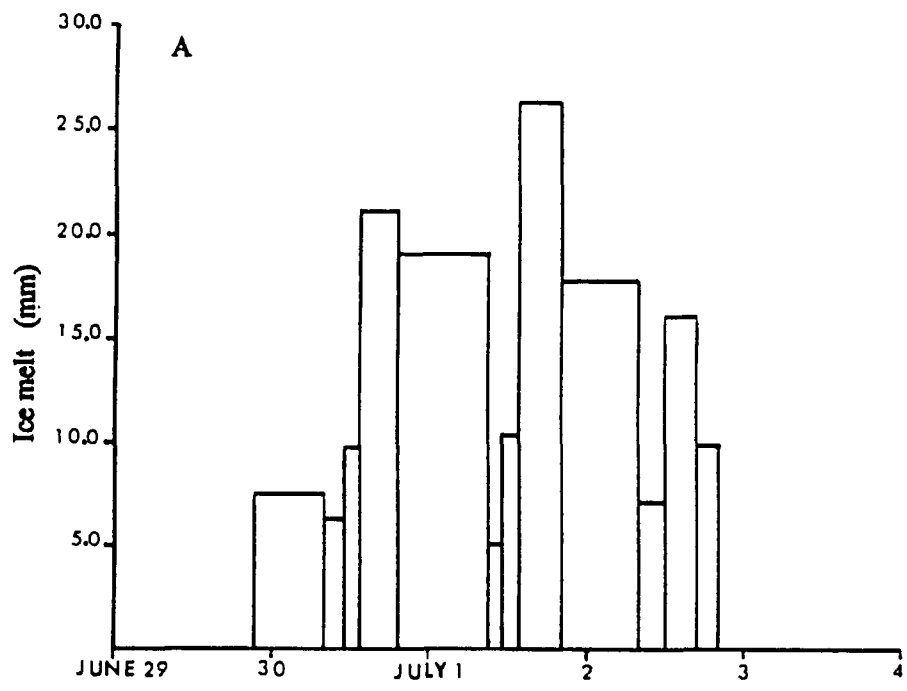
57

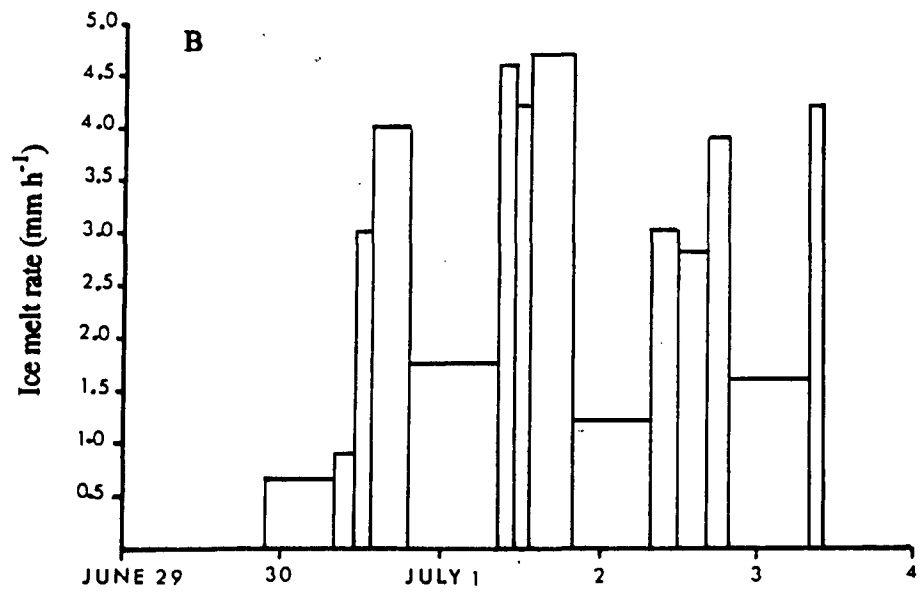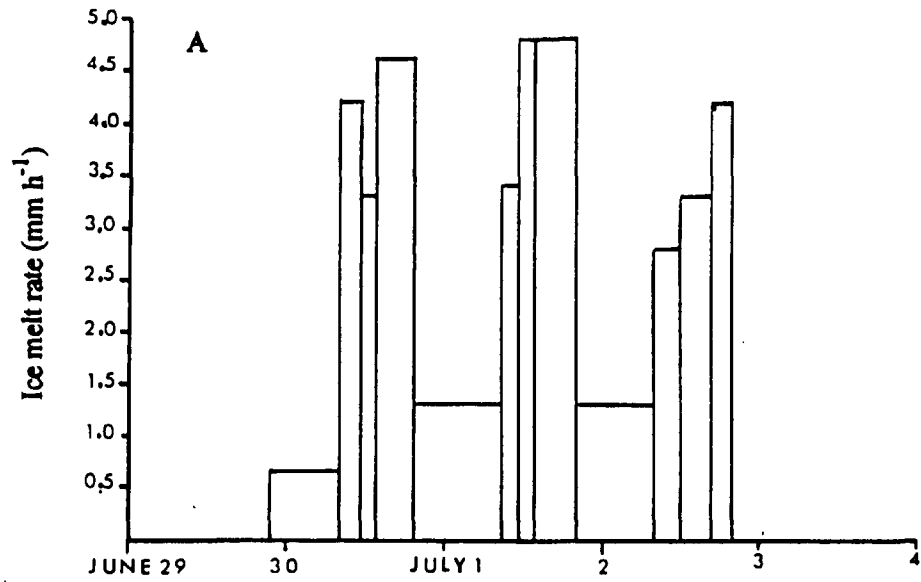Figure 10: Ice melt observed at two locations within Channel Pond.

58

Figure 11: Ice melt rates observed at two locations within Channel Pond.

59

to be much greater than those measured in the Small Lake ice pond. Ice melt rates were found to vary from 0.5 mm h^{-1} to as high as 5.0 mm h^{-1}. The main reason for this difference is primarily attributed to a higher water temperature.

Cross sections of the ice surface are shown in Figure 9c and Figure 12 for both the Small Lake and Channel Pond sites. All of the sites displayed an undulating surface which changed during the study period, probably as a result of variations in the location and strength of convective mixing. This was most pronounced at Channel Pond where initial depressions in the ice surface could end up above the mean ice surface and vice versa. However, once the topographic pattern was firmly established, it tended to remain for the rest of the melt period and local relief increased. At the Small Lake ice pond, an average of 0.035 m of ice melted during the 2 days of study while 0.16 m and 0.18 m of ice were lost at Channel Pond over a three and a half day period.

3.2.3 Water Level and Pond Area

Recorded water levels at the Small Lake ice pond are plotted in Figure 13. The water level decreased each day despite the addition of melt water and the deepening of the pond (Figure 9c). Water was observed seeping into the porous lake ice cover around the pond's margin and flowing downward to the lake level. The area of the pond increased slightly midway through the melt period before drainage reduced the
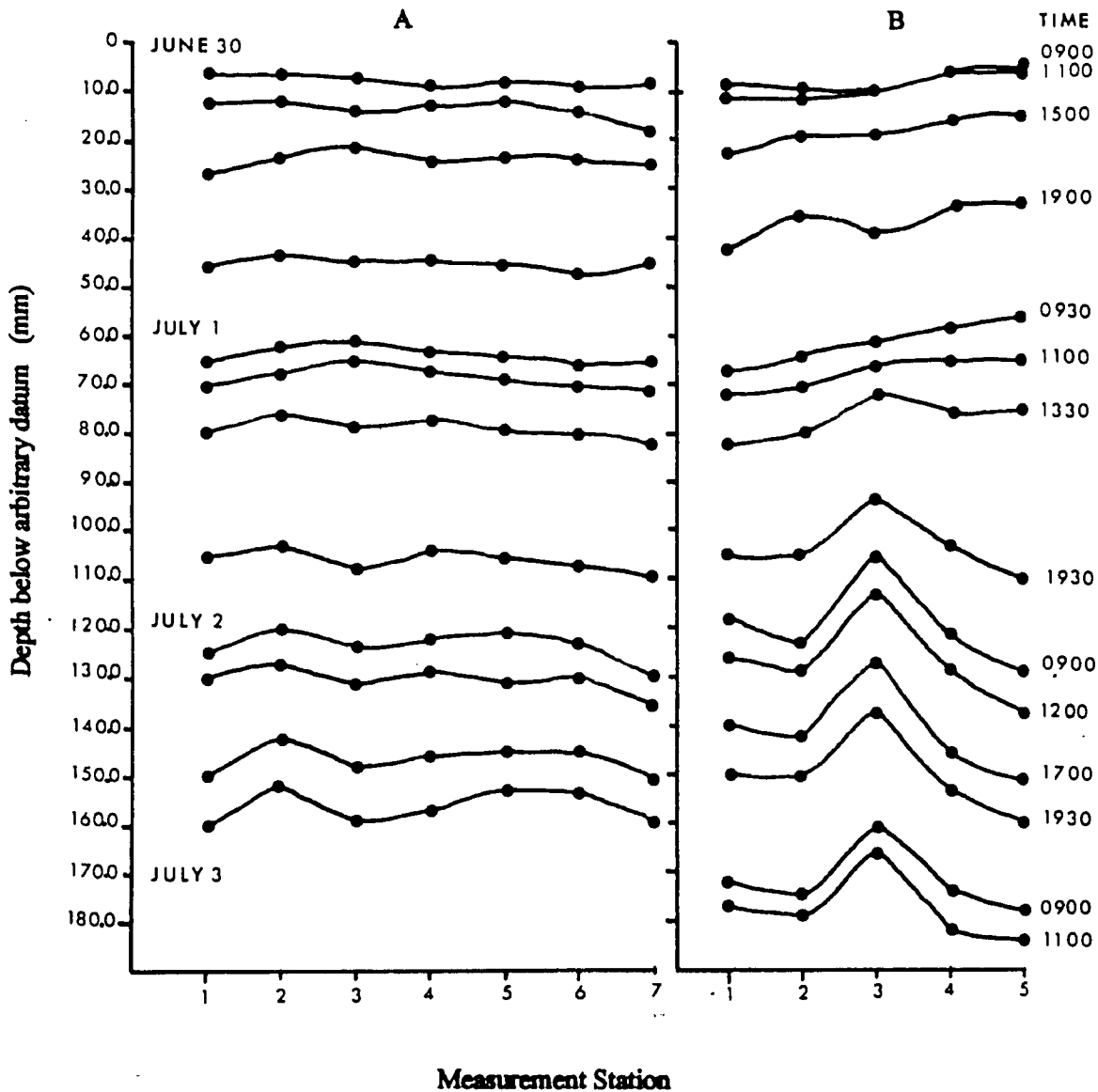
60

Figure 12: Cross sections of the basal ice surface of Channel Pond at two locations showing the evolution of the surface during the study period. Distance between measurement stations is approximately 0.1 m.

Small Lake melt pond
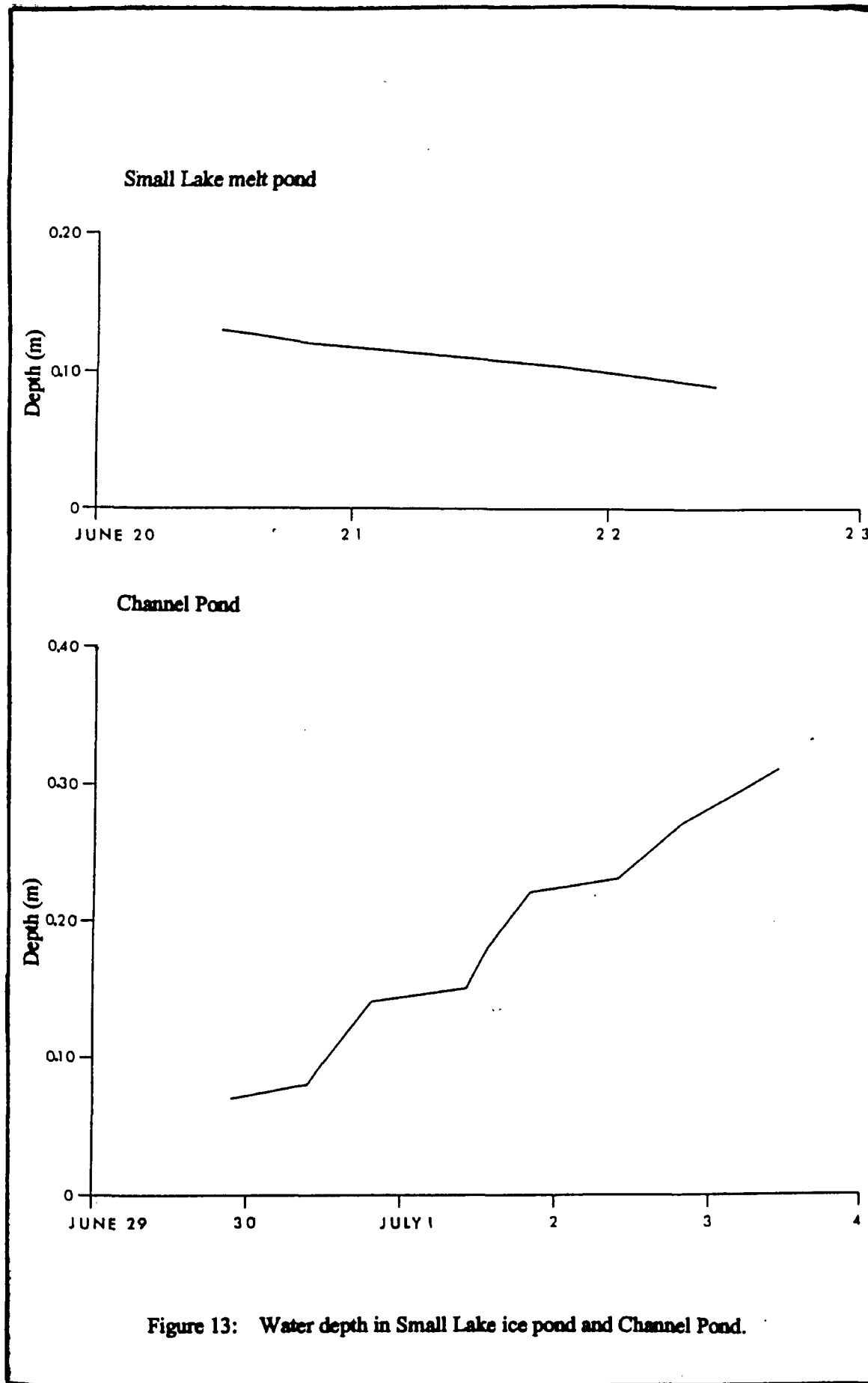
Channel Pond

Figure 13: Water depth in Small Lake ice pond and Channel Pond.

62

pond to the same size as it was at the start of the experiment.

In contrast to the Small Lake ice pond, the water level of Channel Pond continued to increase with time (Figure 13). The data show that water levels increased most rapidly during the day and very slowly during the evening. While much of the increase was produced as a result of the lowering of the basal ice surface, a great deal of meltwater was also added to the pond by snow and ice melt from the surrounding, irregular topography. During the three day experiment, the length and width of the ice pond increased from 70.0 m and 30.0 m to 75 m and 45 m, respectively, as snow drifts filling the pond basin were flooded.

3.3 Computed Energy Fluxes

3.3.1 Net Long-wave Radiation

Net long-wave flux density (L*) is the difference between the atmospheric (L↓) and terrestrial (L↑) long-wave radiation components, and is computed using Equation 14. Net long-wave flux density calculated for both sites are illustrated in Figures 14 and 15. The long-wave radiation balance is negative throughout the periods studied, indicating that the ponds were continuously losing energy to the atmosphere. Because the net-long wave flux density is calculated as a residual, there were considerable fluctuation in the values. However, at both sites there was a diurnal pattern. In the

63
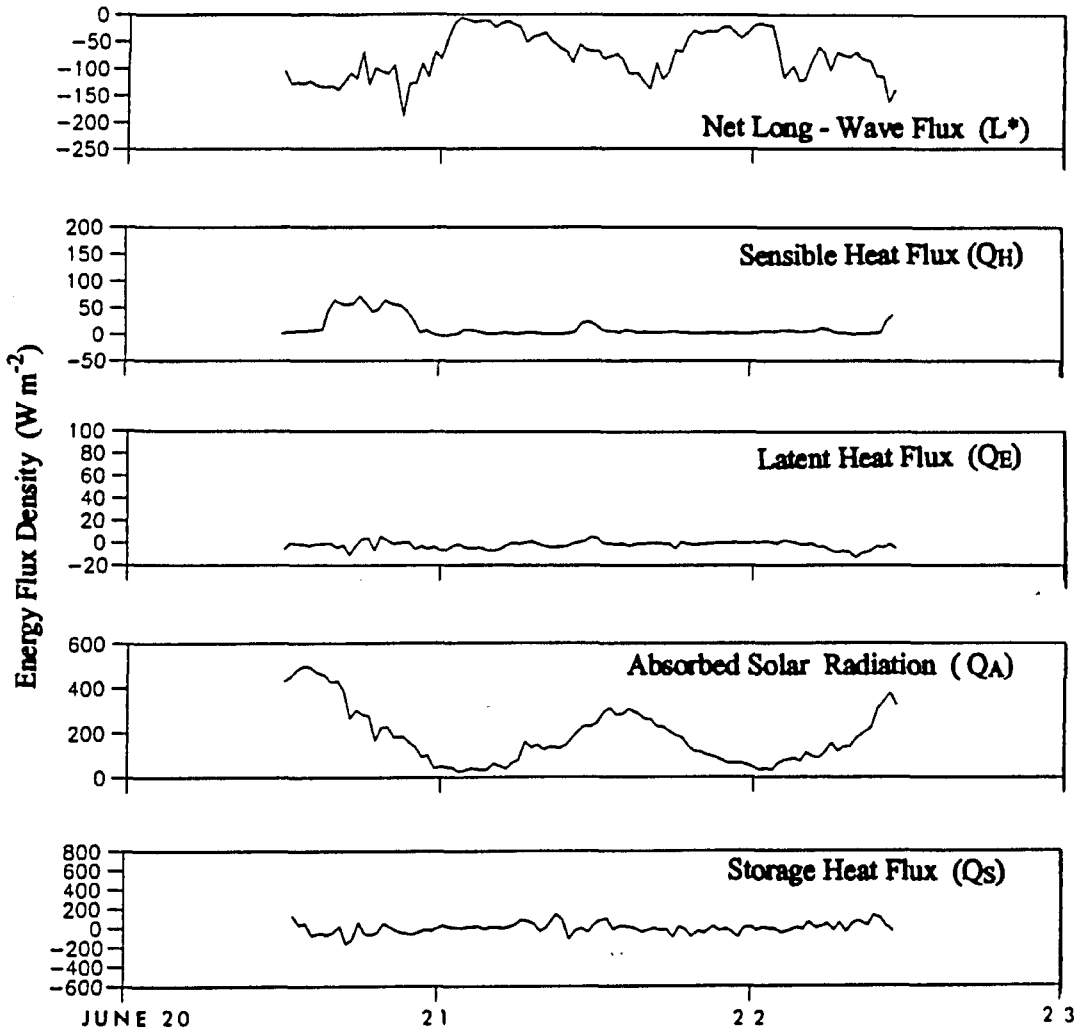
Figure 14: Computed energy fluxes for the Small Lake ice Pond.

64
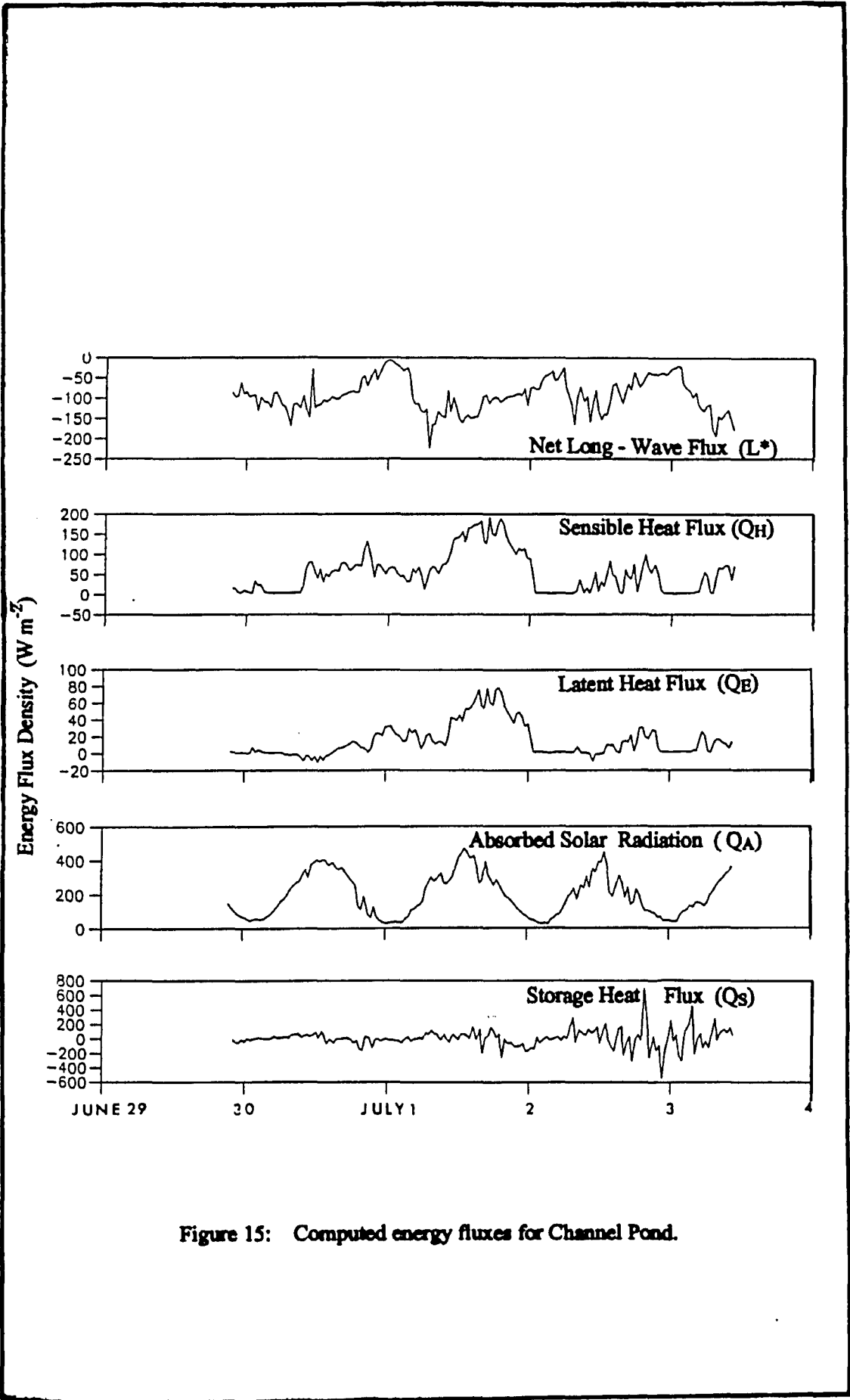
Figure 15: Computed energy fluxes for Channel Pond.

late evening and early morning hours, the ponds were cool and the loss of long-wave radiation was small. With increased pond temperatures during the day, the increased emissions of long-wave radiation from the water decreased the long-wave balance.

The data for each site studied show that approximately 50 to 100 W m^{-2} of total long-wave energy was released into the atmosphere in the early morning and late evening hours. Near or shortly after midday, this total increased to between 150 to 200 W m^{-2}.

3.3.2 Sensible Heat Flux

The flux of sensible heat (Q_H) is the transfer of heat through the process of convection due to surface and air temperature differences. For this investigation, the sensible heat flux was determined using the bulk aerodynamic method (Equation 15). Sensible heat flux estimates made over the Small Lake ice pond and Channel Pond are shown in Figures 14 and 15.

Inspection of the data show that sensible heat flux estimates made over both ponds were positive throughout. When surface and air temperature difference was at a maximum (near midday) and there was sufficient wind, the flux of sensible heat at the Small Lake ice pond was near 80 W m^{-2}. However, when one of these conditions was not met, the flux of sensible heat supplied very little energy to the supra-ice melt pond.

66

Periods of calm are also evident in the sensible heat flux calculated above Channel Pond. However, because of higher air temperate and wind speeds, the sensible heat flux was substantially greater than that observed at the Small Lake site. It was estimated that the flux of sensible heat supplied between 4 and 200 W m^{-2} of energy to Channel Pond.

3.3.3 Latent Heat Flux

The flux of Latent heat (Q_E) is the energy absorbed or released when water evaporates or condenses on the surface. For this analysis, the latent heat flux densities were also determined via the bulk aerodynamic method (Equation 16). Estimates of Q_E made over the Small Lake pond and Channel Pond are found in Figures 14 and 15.

At Small Lake, the latent heat flux density remained small and fluctuated around zero. The maximum and minimum values were -11.0 and 6.0 W m^{-2}. Higher atmospheric humidity during the period over which Channel Pond was examined resulted in the latent heat flux almost always contributing energy to the water. While the minimum flux density was about 11.0 W m^{-2}, high wind speeds on July 1st caused the latent heat flux to reach 80.0 W m^{-2}.

3.3.4 Absorbed Short-wave Radiation

The incoming short-wave radiation absorbed (Q_A) in each supra-ice melt pond was determined by summing the direct and

indirect absorption components (Equation 27).

The amount of solar radiation absorbed by the ponds displayed a diurnal pattern because of the importance of incident solar radiation in determining this component. The flux of absorbed short-wave radiation reached more than 400 W m^{-2} near midday in Channel Pond. Even at night when the sun was low in the sky, absorbed radiation amounted to 25 W m^{-2}.

At the Small Lake site, the flux of absorbed short-wave radiation was reduced due to a smaller flux of incident radiation and thinner water layer. At both sites, most of the radiant energy was absorbed directly with 4.0 W m^{-2} absorbed after short-wave radiation was reflected off the ice-water interface.

3.3.5 Heat Storage

The change in heat storage (ΔQ_S) within each pond was determined by observing the change in water temperature and converting this into an equivalent energy flux density (Equation 28). The change in heat storage in the Small Lake ice Pond and Channel Pond are found in Figures 14 and 15.

The data for the Small Lake site show that the heat storage flux density fluctuated within ± 200 W m^{-2} of zero and had a subtle diurnal cycle. At Channel Pond, the diurnal pattern is more obvious. In general, energy is stored during the late morning and early afternoon hours when total absorbed short-wave solar radiation, sensible heat and latent heat flux

68

estimates are at or near their peak. At night when these fluxes decrease, the heat is released from the water (negative heat flux density) and used to support ice melt and the loss of long-wave radiation.

The daily storage heat flux pattern observed at Channel Pond was consistent until July 2nd. Thereafter, the storage heat flux was highly variable with very numerous large peaks and troughs throughout. This is largely due to rapid variations in the surface energy balance. However, some fluctuations may be the result of ice blocks, released from other parts of the bottom of the pond, floating in the vicinity of the thermistors and cooling the water. The water temperature would rise after wind caused the ice to drift away, thus creating the appearance of a large and rapid change in heat storage in the entire pond.

3.3.6 Heat Flux into the Ice

Some of the energy available to melt ice may instead by conducted into the ice and transferred downward to warm the ice and substrate. Temperature profiles from Heron (1985) indicate that in the initial stage of lake ice melt, the absorption of solar radiation caused near-surface ice layers to be isothermal. Under these conditions, the heat flux into melting lake ice from the surface will be zero. However, where lake or pond ice remains frozen to the bed for some time, the ground heat flux must be considered. For this

reason, an attempt was made to estimate the ground heat flux (Q_G) into the ice substrate of Channel Pond. The initial temperature profile used in this analysis was based on Marsh (1984) and Heron (1985) and the successive ice temperatures were modelled using the explicit numerical scheme outlined by Fertuck et al. (1971) and the observed environmental conditions.

The simulated temperature profiles are illustrated in Figure 16. The temperature profiles generated during July 1st were selected because it provided sufficient time for the temperature profile to stabilize under natural conditions. In all cases the temperature profiles display isothermal conditions in as much as the top 0.15 m of the ice, and somewhat less at night.

Given that an isothermal condition was calculated for the ice layers below the ice-water interface, the ground heat flux in Channel Pond was ignored in the energy balance and ice melt calculation.

3.3.7 Energy Flux Used to Melt Ice

To compute the energy flux used to melt the basal ice surface of each supra-ice melt pond, an estimate of ice density was required, in addition to the measured ice melt rates. During the ground heat flux calculations above, it was evident that more short-wave radiation was absorbed in the ice than necessary to produce an isothermal profile. This excess
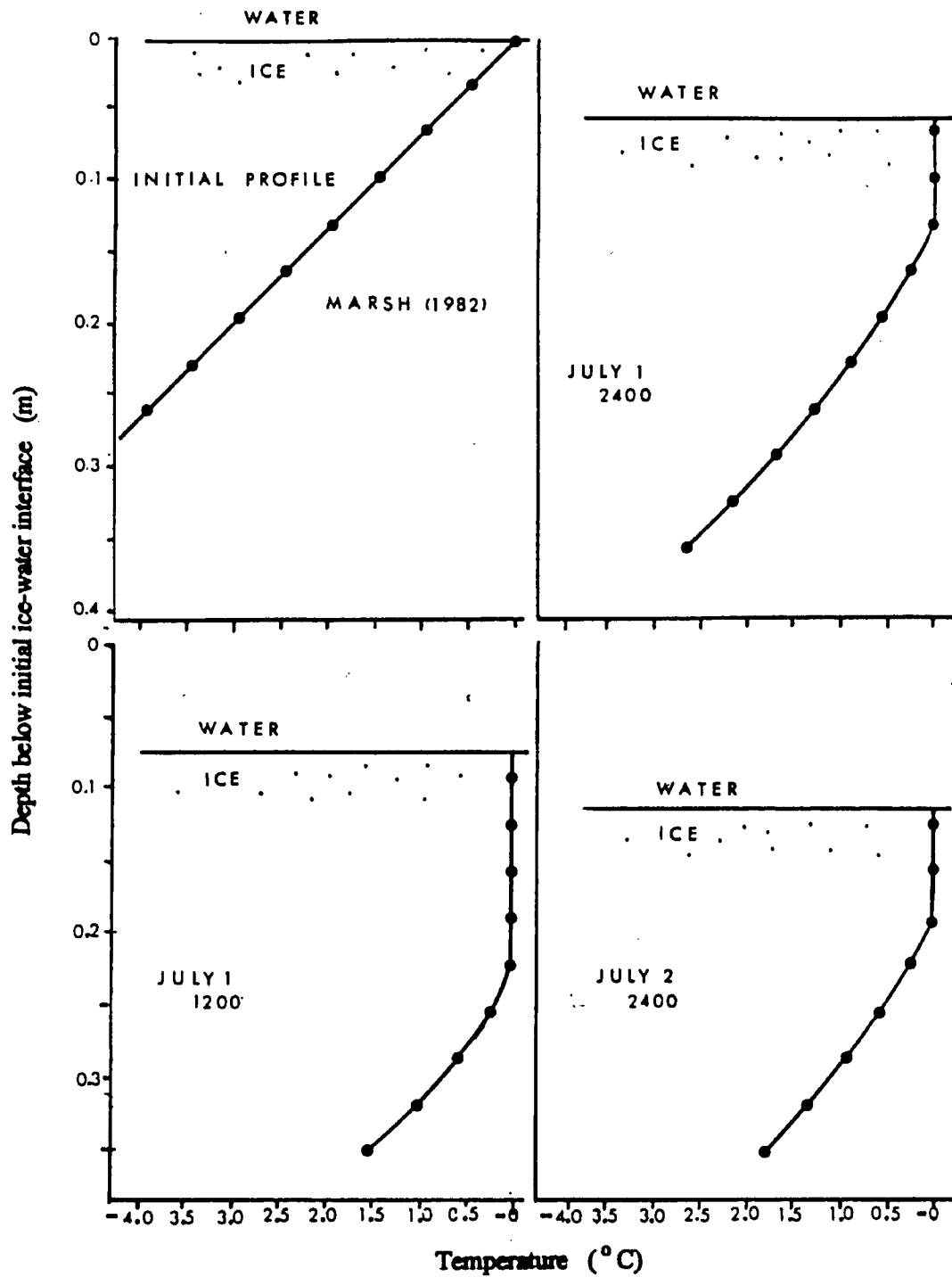
70

Figure 16: Selected simulated ice temperature profiles for the ice at the base of Channel Pond

71

energy causes melting within the ice, increasing its porosity and decreasing its density from the point of view of Equation 5. The extra energy was accumulated for each layer and multiplied by the ratio of density of solid ice to the energy required to complete melt to an equivalent layer of solid ice.

After making an allowance for air bubbles in the ice, an ice density of 830.0 kg m^{-3} was used for Channel Pond and 890.0 kg m^{-3} for the Small Lake ice pond. The energy allocated for ice melt in the Small Lake ice pond and Channel Pond are displayed in Figure 17.

The greatest melt rates were observed during the day when energy was abundant while decreasing at night. Because the ground heat flux was zero, the ice was unable to grow upward and only melt was possible. The energy flux used to melt ice ranged from 50.0 to 400.0 W m^{-2} at Channel Pond and between 40.0 and 170 W m^{-2} at the Small Lake ice pond.

3.4 Diffusivity

3.4.1 Interfacial Thermal Diffusivity

The interfacial diffusivities for both sites are presented in Figures 18 and 19. The smallest value was 1.38 x 10^{-7} m^2 s^{-1}, about the same as the diffusivity of still water, 1.44 x 10^{-7} m^2 s^{-1}. Most of the values from both ponds were less than twice the value of still water while the largest one was just over 4 times larger. The lowest layer of Channel Pond displayed a diurnal cycle with thermal
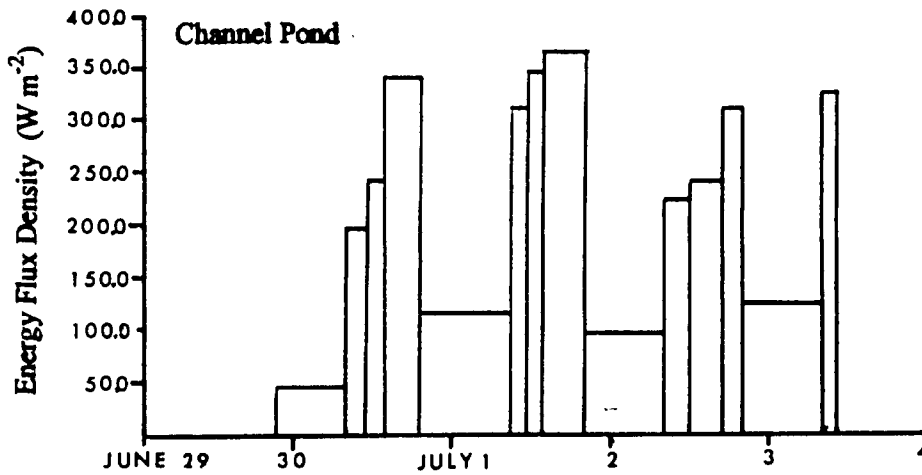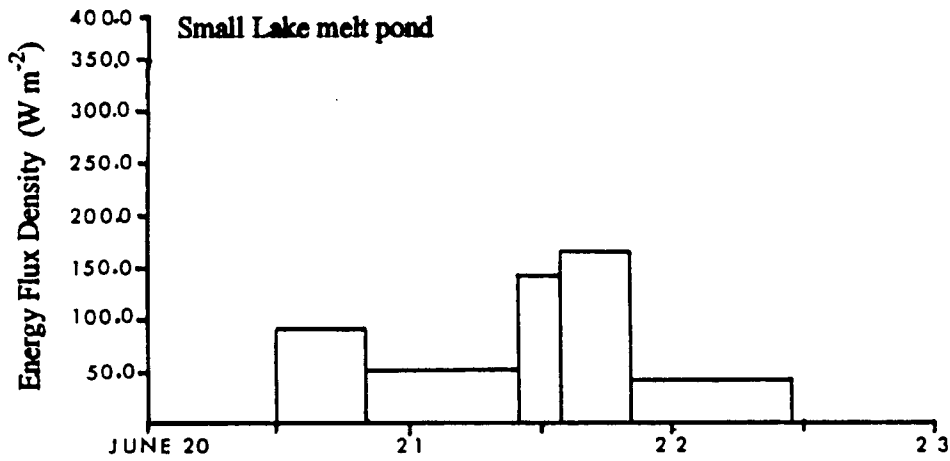
72

Figure 17: Energy flux used to melt ice at the base of the Small Lake ice pond and Channel Pond.

73
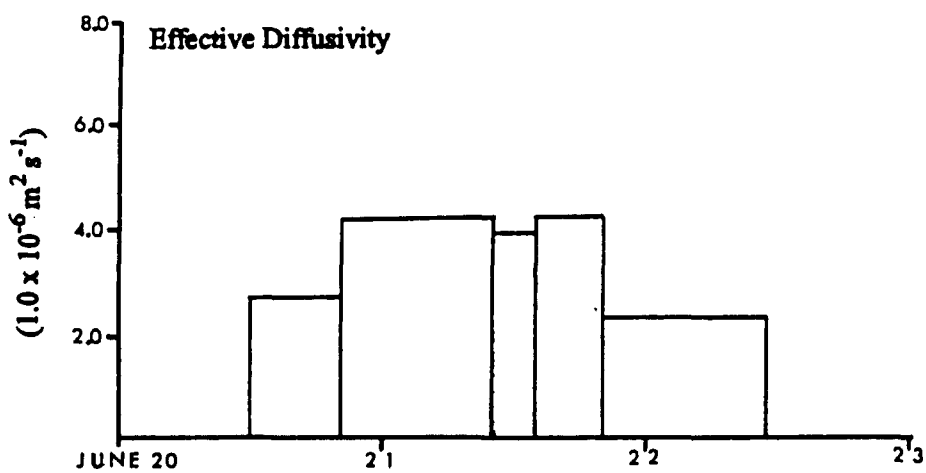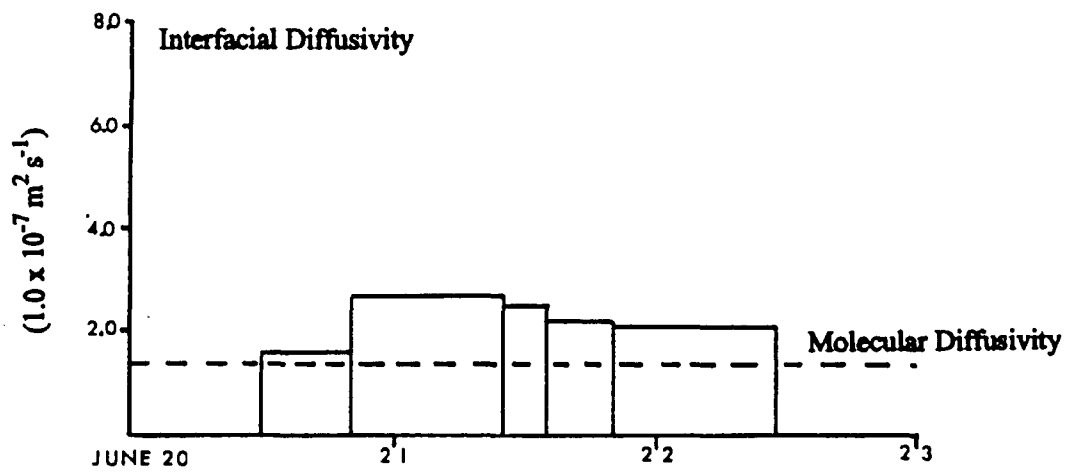
Figure 18 : Interfacial and effective vertical thermal diffusivity for the Small Lake melt pond.

74
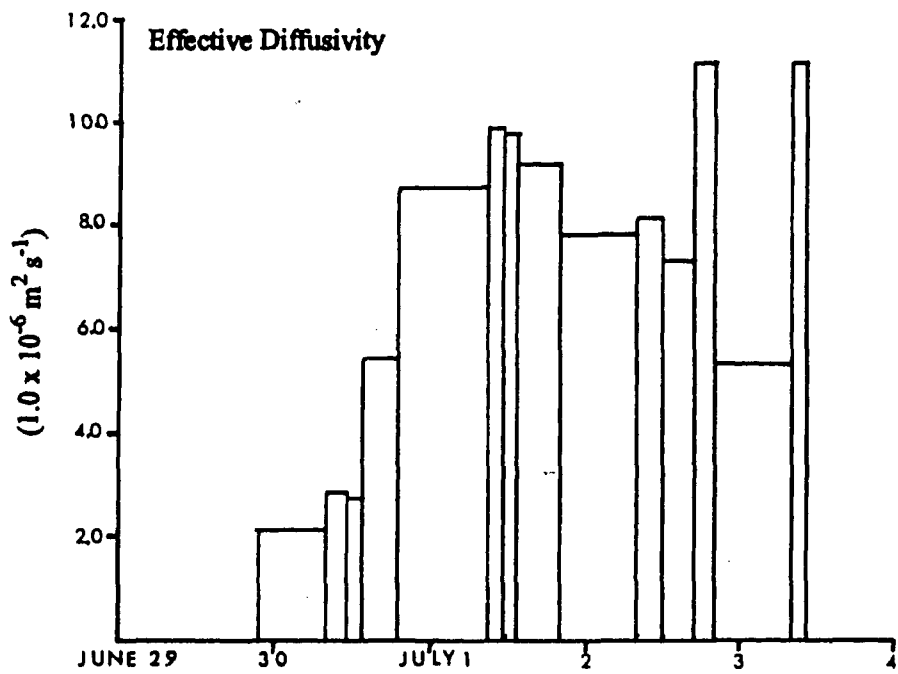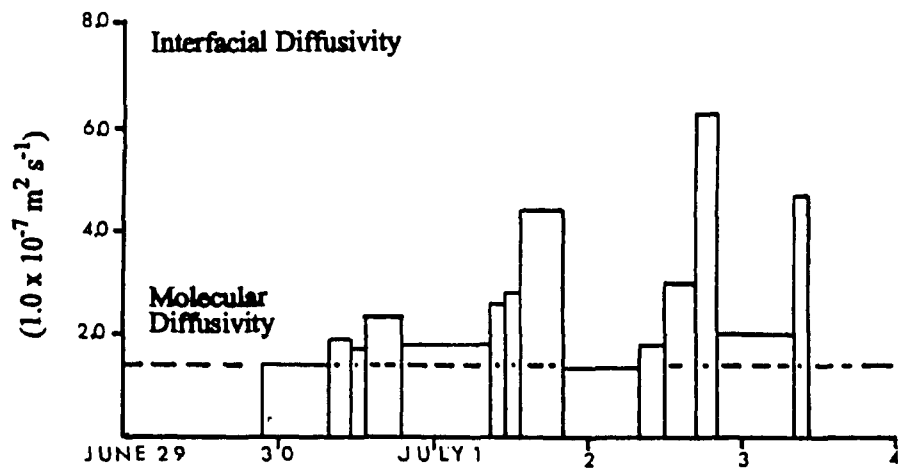
Figure 19: Interfacial and effective vertical thermal diffusivity for Channel Pond.

75

diffusivities peaking during the afternoon and declining to near still water values at night. This was not noticeable at the Small Lake site, possibly because of the longer measurement periods and cooler water temperature. The fact that the smallest thermal diffusivities of the lowest pond layer are similar to the thermal diffusivity of still water supports the decision not to allocate any absorption of radiant energy to the ice surface. If it were included, the diffusivities would be less the value for still water, which is not possible.

The peak thermal diffusivities are probably overestimated by up to 15 %. Since the thermistors were supported from above by the instrument platform, the ice surface melted during the afternoon, and the thermistors occasionally moved upward relative to the ice surface, into water a few tenths of a degree warmer. Although the distance above the interface was left at a nominal 0.005 m, this temperature difference could increase the temperature gradient by about 10 to 15 % given typical water temperatures.

3.4.2 Effective Thermal Diffusivity

The apparent or effective thermal diffusivities for the Small Lake site and Channel Pond are shown in Figures 18 and 19. The calculated values ranged between 2.09×10^{-6} m^2 s^{-1} and 11.9×10^{-6} m^2 s^{-1}, between 1 and 2 orders of magnitude greater than the value for still water. These values are in the same

76

range as the diffusivities used by Wake and Rumer (1979) for their simulations. The diurnal pattern observed for the Channel Pond interfacial thermal diffusivities are no longer as visible, possibly being overwhelmed by other important factors such as wind-induced mixing and water depth.

Wake and Rumer (1979) suggested that there are a number of environmental variables such as wind and water depth that could alter the effective vertical thermal diffusivity coefficient in an air-water-ice system. To investigate this possibility, a step-wise linear regression analysis was employed to select the most appropriate combination of independent variables, water depth, water temperature, and wind speed, needed to explain the variation in diffusivity. Using the statistical package SYSTAT, it was determined that wind speed and water depth provided the best results with water temperature being of no value in predicting diffusivity. The correlation coefficients between effective diffusivity and water depth and effective diffusivity and wind speed were 0.915 and 0.817, respectively.

A multiple linear regression analysis was then employed to determine how water depth and wind speed influenced effective diffusivity, the dependent variable. A number of assumptions regarding this statistical technique need to be met before the relationship could be considered valid (Clark and Hoskings, 1986). The results of this analysis showed that the independent variables were not collinear with one another

and the residuals from the regression equation were found to be homoscedastic. In addition, the Durbin-Watson test also indicated that there was no first-order autocorrelation present in the residuals. The regression equation predicting the effective thermal diffusivity (D_w) was:

$$D_w = 9.99 \times 10^{-7} \, (U_a) + 2.53 \times 10^{-5} \, (h)$$

(Equation 37)

where wind speed (U_a) and water depth (h) are measured in m s^{-1} and m, respectively. This statistical relationship provided a significant Pearson's "r" coefficient of 0.975 and a coefficient of determination "r^2" of 0.947. Thus 94.7 % of the variation in the effective thermal diffusivity can be attributed to wind speed and water depth. This equation appears reasonable since higher wind speed should be expected to increase the mixing of the water column and as the depth increases, the diffusivity must increase to compensate for the decreased temperature gradient.

78

CHAPTER 4

DISCUSSION AND CONCLUSIONS

One aim of this thesis was to examine the characteristics and processes operating in a supra-ice melt water pond, since virtually no information is available in the literature. This included not only the water temperature and ice melt rate, but also the energy exchanges above, within and below the pond. Since there were no independent values with which to compare each of the energy exchanges, the only available check is the energy balance. While this will not verify the energy transfers, major errors may be identified if the balance residual is large.

4.1 Energy Balance

To calculate the energy balance (Equation 1) for Channel Pond and the Small Lake ice pond, the flux density (W m^{-2}) of each energy component was converted into an equivalent energy total (MJ m^{-2}) for each ice melt period and summed for the study period. The magnitudes of these components and the residual balance error term are given in Table 2.

The results for the Small Lake ice pond show that absorbed radiation (Q_A) and sensible heat flux density (Q_H)

79

Table 2: Energy balance totals for the Small Lake ice pond and Channel Pond.

Energy Flux (MJm^{-2})	Small Lake Total Period	Small Lake Revised Period	Channel Pond
Q_A	31.05	19.82	59.18
Q_H	2.13	1.04	16.42
Q_E	-0.31	-0.28	4.58
ΔQ_S	0.04	0.69	3.01
L^*	-12.94	-9.47	-28.74
Q_M	-13.09	-10.32	-52.64
Residual Energy	6.88	1.48	1.81
Measurement Duration of Study (Hours)	47.5	39.0	85.5

80

are the largest producers of melt energy while the principle consumers of this energy are net long-wave flux density ($L*$) and the energy flux used to melt the basal ice surface (Q_M). In addition to the larger energy consumers, some energy was also removed via the latent heat flux density (Q_E). The amount of energy lost through evaporation however, was considerably smaller in comparison to the other energy consumers.

Since all of the energy transfer terms in Equation 1 were measured or calculated independently, it is possible to obtain the residual balance term, which should ideally be zero. The sum of the energy exchanged by each process shows that there is some error in the above terms since energy gains exceed the losses. In the case of the Small Lake site, the residual energy for the entire study period is very large. Most of the error appears to be due to the data collected during the first observation period, probably owing to an overestimate of absorbed radiation (Q_A) as a result of instrument levelling problems. Other components such as ice melt (Q_M) or sensible heat flux (Q_H) density may have also contributed. When the results of the first measurement period are removed, the revised energy balance still shows an energy surplus but it is reduced from 6.88 MJ m^{-2} to a more reasonable 1.48 MJ m^{-2}.

The energy balance of Channel Pond shows the same basic trend as noted above. The greatest producers of melt energy were absorbed radiation (Q_A) and sensible heat flux density

(Q_H), while net long-wave flux density (L*) and the energy flux density used to melt basal ice (Q_M) were the greatest consumers of this energy. Unlike the Small Lake ice pond, the latent heat flux density (Q_E) was an energy producer due to condensation on the pond surface, rather than evaporation. While the sign was different, the magnitude of the latent heat flux density (Q_E) was still small in comparison to the sensible heat flux density (Q_H) and absorbed radiation flux density (Q_A,) but similar to that of the storage heat flux density (ΔQ_S). At both sites, the ponds had a net increase in the amount of heat stored due to a slight increase in water temperature, as well as an increase in water depth in the case of Channel Pond.

The residual error component for Channel Pond is small and indicates an excess of energy. However, some of the energy in the balance residual for both sites includes heat that was lost when water seeped out of the ponds, but was not accounted for.

To allow comparisons to be made between study sites, the energy balance components (Table 2) were converted to a percentage of total available energy (Table 3). The data show that net radiation (Q*) supplied 75 % and 55 % of the total energy needed to melt the Small Lake and Channel Pond ice surfaces, respectively. At Channel Pond, favourable water temperature, wind speed and humidity conditions permitted the sensible heat flux density (Q_H) to supply 29 % of the total

82

Table 3: Comparison of the relative contribution of the energy exchange components at Small Lake ice pond and Channel Pond with other studies.

Study	Location	Site	Q* (%)	Q_H (%)	Q_E (%)	Q_M (%)	Q_S (%)	Q_P (%)	Error
This Study (1992)	Resolute	Small Lake	76	8	-3	-97	5	—	11
		Channel Pond	55	29	8	-100	5	—	3
		Average	65.5	18.5	2.5	-98.5	5	—	7
Granger and Male (1977)	Sask. (1974) (1975) (1976)	Snow Snow Snow	59 95 54	41 5 46	-14 -22 -15	-86 -78 -58	— — —	— — —	— — —
Heron (1978)	Resolute (1977)	Snow	60	40	—	-100	—	—	—
Braitwaite (1981)	White Glacier (1960) (1961) (1962) (1963)	Axel Heiberg Devon Island	55	34	11	100	—	—	—
Heron (1985)	Resolute (1980) (1981)	(Small Lake) Bare Lake Ice	46 45	47 42	7 13	-100 -100	— —	— —	— —
Hay and Fitzharris (1988)	New Zealand	Ivory Glacier	52	34	12	-100	—	2	—
Munro (1990)	Alberta	Peyto Glacier Ice Snow	65 51	34 42	1 7	-100 -100	— —	— —	— —

melt energy while at the Small Lake ice pond, the sensible heat flux density (Q_H) only contributed 8 % of the total energy. A comparison of the latent heat flux densities (Q_E) show that this energy component is very small and fluctuates slightly above (energy source) and below (energy sink) zero. The data from the two studies also clearly illustrate that almost all of the energy entering into the ice ponds is used to melt ice. While some energy is also stored within the water portion of each ice melt pond, the data show that this energy component is very small and near the latent heat flux estimates. Finally, the residual balance or error term for Channel Pond is only 3 % while the Small Lake melt pond has an balance error of 11 %. Both of these values are acceptable considering the simplifications and assumptions required to determine the energy fluxes.

Given the lack of energy balance results for supra-ice melt ponds, the results of both sites were averaged and compared to energy balance studies conducted on glacial ice, lake ice, sea ice and snowpacks (Table 3). In general, the data for this study compares favourably with other results. While the percentage contribution of each component varies between studies, the data obtained in this project follows the same basic trend. However, because of the water layer, the manner in which the energy is transferred is much different.

84

4.2 Water Temperature and Heat Flow

The unique aspect of the energy exchange of melt ponds is the role of water in transferring heat to the underlying ice. Water temperature profiles for all but the interfacial layer above the ice were nearly isothermal (apart from measurement and calibration errors) indicating that convection was rapidly moving heat to and from the water surface. During the day when the water surface had a surplus of energy, the water temperature occasionally decreased with depth and at night the temperature gradient reversed slightly to provide heat to the water surface.

The laboratory results are consistent with the observed results in some respects, but differ in other ways. While all studies have reported the isothermal convective layer, many, especially Townsend (1964) Adrian (1975) and Yen (1980), have noted that water temperature regularly increased by about 0.3 °C with depth in the 'isothermal' layer. The explanation was that water between 3.2 and 3.98 °C was subsiding to the base of the convecting layer and the rising of plumes of less dense, but colder water, were slowed once they hit the stable layer of water, where temperatures were above 3.98 °C, and overlay the convecting layer. Since neither the stable layer or water above 3.2 °C were observed in this study, an increase in temperature with depth was only observed at night and was due to a negative water surface energy balance causing the

85

surface to cool.

The only examples of water temperature decreasing with depth in the mixing layer in the literature are provided by Lunardini et al. (1986). In that case, water was allowed to cool to temperatures comparable to those in this study and the only source of energy to melt ice was moving downward from heat stored in the water. Much of the energy to warm the water in this study came from radiation absorbed within the water column and although the water surface was receiving some energy it was small in comparison to most of the other laboratory experiments.

The mean temperature of the convective layer reported in the literature ranged from 2.85 °C (Adrian, 1975) to 3.2 °C (Townsend, 1964; Yen, 1980) and 3.4 °C (maximum) (Lunardini et al., 1986). In this study, the temperatures varied from 0.2 °C to a maximum of 2.6 °C due to the limited energy available. It is not known if a stable layer (with temperatures greater than 3.98 °C) would have started to form at the water surface, above the isothermal convective layer, if additional energy was available to increase temperatures to 3.4 °C, or whether the isothermal layer would continue to warm to 3.98 °C, before the stable layer formed.

Laboratory studies have shown that between the ice surface and the isothermal stratum was a layer in which convective mixing was damped out and molecular diffusion ultimately transferred all heat to the ice surface. This

layer, typically less than about 10 mm thick, was marked by a very steep temperature gradient near the ice surface which gradually decreased with distance away from the ice-water interface. While the temperature profiles obtained in this study lack the spatial resolution to provide details of this layer, they do confirm its presence and approximate thickness.

Both laboratory results and the observations of this study differ greatly from the predicted water temperature profiles of Wake and Rumer (1979), who assumed no vertical mixing in their ice melt model. As a result of using the thermal diffusivity that was held constant with depth, they obtained quasi-linear water temperature profiles with surface temperatures of up to 6.0 $^{\circ}$C. When a thermal diffusivity two orders of magnitude greater than the value for still water was employed, a more reasonable, but somewhat low, surface temperature of 0.6 $^{\circ}$C was achieved with their assumed atmospheric conditions. Clearly, using a thermal diffusivity value that is constant with depth will not produce the temperature profiles observed in either this study or the relevant parts of the laboratory results.

In their laboratory experiment with still water, Lunardini et al. (1986) obtained a linear relationship between the water heat flux to the ice (Q_w) and temperature difference between the bulk water and the ice surface (ΔT) when the water temperature was less than 3.4 $^{\circ}$C. The empirical equation obtained from this relationship is

87

$$Q_w = 135.7 \, \Delta T \hspace{4cm} \text{(Equation 38)}$$

Above this critical temperature, the heat flux was unstable but varied about a mean rate of 488.5 W m^{-2}. The results of this study are plotted in Figure 20 along with Equation 38. The Small Lake ice pond results agree very well with the laboratory derived relationship, probably owing to the rather low wind speeds throughout the two day period. However, for Channel Pond, only half of the values conform to the linear relationship. In general, when the heat flux is greater than 300 W m^{-2}, the results are substantially greater than those predicted by bulk water and ice temperature differences alone. All of these outlying points have average wind speeds between 2.1 and 4.6 m s^{-1} while the average wind speed of the points near Equation 38 in Figure 20 is less than 2.6 m s^{-1}. This result suggests that wind is increasing the rate of heat transfer and that it does not become dynamically significant until a critical wind speed has been reached.

4.3 Vertical Thermal Diffusivity and Heat Transfer

On a number of occasions, the interfacial thermal diffusivity values for both melt ponds were essentially the same as the molecular thermal diffusivity (Figures 18 and 19). Since the interfacial thermal diffusivity cannot be less than the molecular rate, this implies that the layer of water
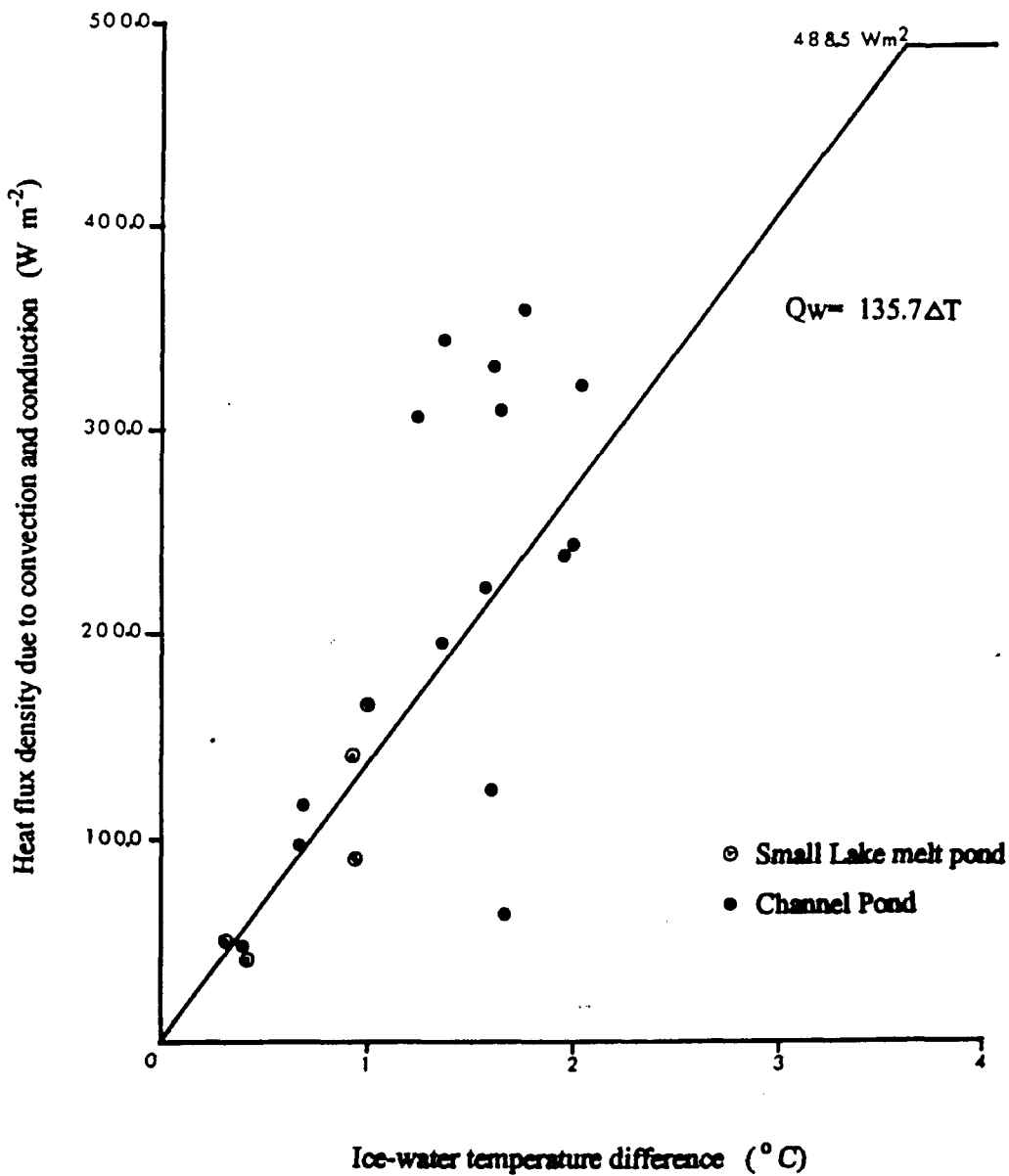
88

Figure 20: A comparison of measured heat flux water temperature relationship from the laboratory experiment of Lunardini et al.(1986) to the Small Lake and Channel Pond results.

89

immediately above the ice-water interface is still. Given the distance of the lowest thermistor above the ice surface, this layer of still water is at least 5 mm thick at night when the water heat flux (Q_W) arriving at the ice surface is low. However, many calculated interfacial thermal diffusivities exceed the still water value by up to four times. While it may seem as if the transition layer between the ice and the convective water layer was slowly mixing, the layer of still water became thinner and the temperatures measured at 5 mm included water from the convective layer. Adrian (1975) indicates that the thickness of the water layer in which heat flows only by molecular conduction is inversely proportional to $Q_W^{0.4}$.

The effective thermal diffusivity for the entire water thickness was found to be a function of both wind speed and depth (Equation 37). While its effect is represented in a linear manner in this equation, Figure 20 suggests that winds, above a speed of about 2.1 to 2.6 m s^{-1}, may be most important. Wind can affect the heat transfer through the water in several ways. The orbital motion of the water beneath the surface may assist the convective mixing and if the waves are large enough, relative to the water depth, this motion may impinge upon the layer of still water above the ice surface, thinning it and increasing both the heat flow and the effective diffusivity. In addition, horizontal circulation may also be established within the pond.

90

Since most of the melt water above the interfacial layer is isothermal, increasing the depth at which the temperature is measured will reduce the temperature gradient to the ice surface. If the heat flux remains constant, then Equation 30 indicates that the thermal diffusivity (thermal conductivity) must be increased. This can be illustrated by substituting a wind speed of 0 m s^{-1} and the thermal diffusivity of still water into Equation 37. Solving for h yields a value of 5.4 mm, which roughly corresponds to the thickness of the still water layer against the ice. From the point of view of the heat flux arriving at the ice surface, the vertical mixing of the ponded water is not important if the surface temperature, depth and effective thermal diffusivity are used to calculate the heat flow. In other words, since the slowest rate of heat exchange is occurring at the molecular rate in a thin layer immediately above the ice cover, it is the thickness of the molecular conduction layer above the ice that ultimately controls the rate of heat flow. Although the effect of the still water layer is hidden in Equation 38, it can be determined by equating the common terms of Equations 36 and 38:

$$135.7 = C_w \, D \, / \, \Delta z \qquad \text{(Equation 39)}$$

Using the thermal diffusivity of still water and solving for Δz gives a conduction layer thickness of 4.2 mm. Equation 38

91

does an good job of describing the data obtained in this study, because the thickness of the conduction layers behaved in a similar manner and were essentially equal. However, if anything, such as wind induced currents, alters the thickness of the layer of water above the ice where heat is transferred by molecular conduction, then the heat flux (for a given temperature) will also change. This may help to explain why the outlying points fall so far from so far from Equation 38.

4.4 Ice Melt Rate and Melt Prediction

The ice melt rates measured in this study ranged from 0.5 to 5.0 mm h^{-1}. These values encompass the range reported by Untersteiner (1961) (0.78 mm h^{-1}, summer average for a sea ice melt pond), Heron (1985) (1.25 mm h^{-1}, Small Lake shore lead) and Lunardini et al. (1986) (<1 to 4.6 mm h^{-1}, still water in an open flume). These are slightly less than the maximum average melt rates for solid ice of 5.6 mm h^{-1} Yen (1980) and 5.7 mm h^{-1} (Lunardini et al., 1986) measured in freely convecting ice-water systems being driven at the maximum rate. The maximum melt rate in this study approaches the maximum values more closely than it should because of the almost 10 % reduction in ice density caused by air bubbles and internal melting.

While two of the stated aims of this project were to obtain estimates of the vertical thermal diffusivity and determine their variability with environmental conditions, the

92

unstated goal was the prediction of the ice melt at the bottom of a melt pool. Now that this study has provided a method of estimating the effective thermal diffusivity, the Wake and Rumer (1979) one-dimensional ice dissipation model can be used to determine ice melt. Although the model is not capable of predicting the water temperature profile, the surface temperature and melt rate should be reasonable. The results of this study also indicate that the model should be modified in several ways. Wake and Rumer (1979) assumed that the conduction heat flux into the ice cover was zero and this was confirmed by this study. However, there are situations where this energy flux may be important (for example, glaciers and sea ice), so it should be added to the model. The results of the interfacial thermal diffusivity calculations suggest that no short-wave radiation was absorbed by the ice surface, otherwise the diffusivities would be less than the minimum possible molecular rates. However, radiation absorption should be included in the basal ice layer since it contributes to the ice surface lowering through internal melting which reduces the effective ice density. The ability of the Wake and Rumer (1979) model to predict ice melt was not tested since the original computer code employing an implicit finite difference scheme was not available and it was beyond the scope of this thesis to reconstruct it.

However, the results of this study and those of Lunardini et al. (1986) indicate that a simpler method is available to

93

predict ice melt if measurements of water temperature are available and the heat conducted into the ice is negligible. Equation 38 can be used directly, or an alternative approach is to incorporate the effective thermal diffusivity equation (Equation 37), which takes into consideration wind speed and pond depth effects, into Equation 36 to estimate the heat flowing through the water to the ice surface.

$$Q_M = C_w [9.99 \times 10^{-7} (U_a) + 2.53 \times 10^{-5} (h)] T_{ws}/h$$

(Equation 40)

Both of these approaches are much simpler than the Wake and Rumer (1979) model and it would be easier to incorporate into a general ice melt model if an estimate of the water temperature is available. The predicted melt energy from both of these approaches is plotted against the measured ice energy in Figure 21. Both methods reasonably predict most of the observations, however there are a number of values which are poorly predicted. It was hoped that the inclusion of wind speed in the estimation of the effective thermal diffusivity would overcome the difficulties with Equation 38 noted earlier, but this did not happen. While the regression analysis showed that wind speed did influence the thermal diffusivity, it may be that the limited sample size of high winds and the relatively long measurement period may have limited the regression results. Given the limited size of the
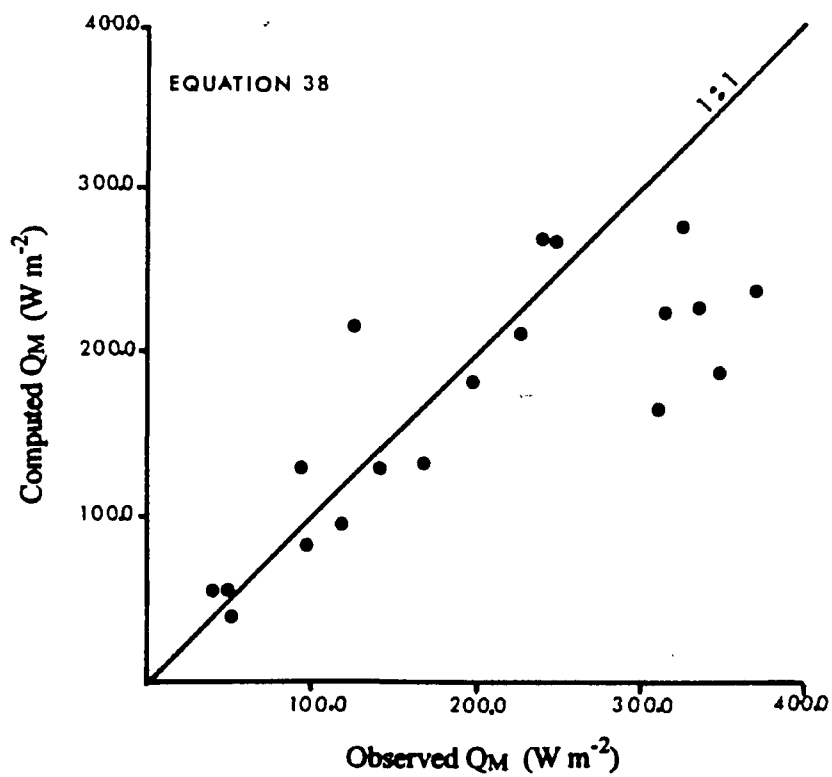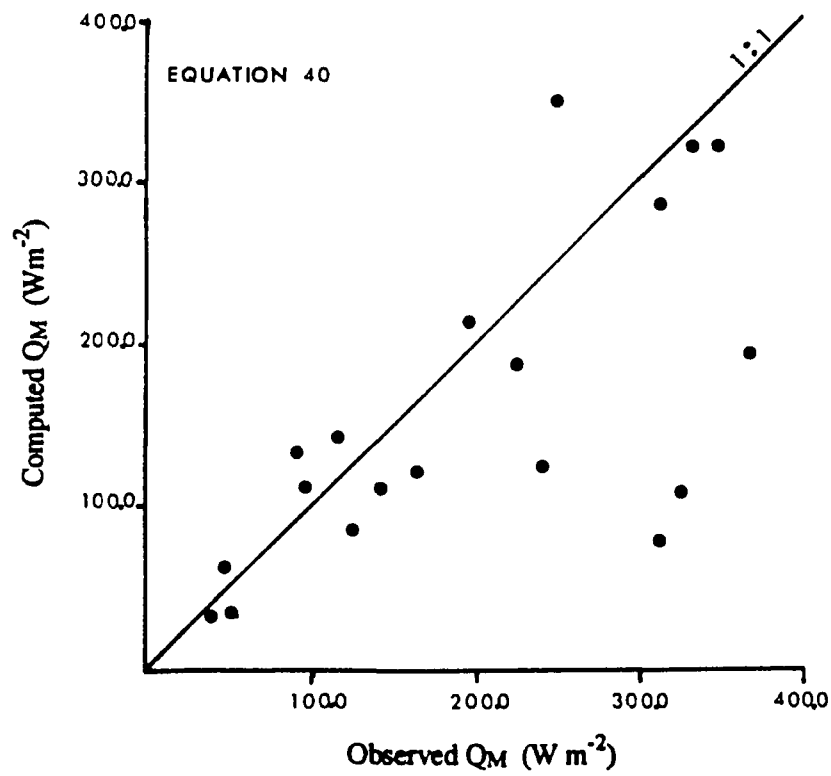
94

Figure 21: Comparison of observed ice melt energy and energy predicted from two different equations.

95

total sample (19), additional data are required to further refine the empirical relationship.

96

4.5 CONCLUSION

The supra-ice melt ponds examined in this study were typical of other fresh-water examples observed in the study area and possessed a similar depth, albedo and melt rate as ponds that form on sea ice. Net radiation ($Q*$) and the flux of sensible heat (Q_H) provided 65.5 and 18.5 % of the total available energy while melt consumed 98.5 %. There was no flux of heat conducted downward through the ice from the ice-water interface.

The water temperature profiles displayed two distinct layers: 1) an near-isothermal, upper layer that included most of the vertical profile and was subject to convective mixing, and 2) a thin layer, just above the ice surface which had a steep temperature gradient where heat was transferred by conduction and some convection. These findings are generally consistent with the results of laboratory experiments. The thermal diffusivity of the interfacial layer was found to be close to the rate for still water. The effective thermal diffusivity, as required in the Wake and Rumer (1979) ice melt model, was between 1 and 2 orders of magnitude greater than the diffusivity of still water. A regression and correlation analysis showed that the effective diffusivity varied with water depth and wind speed ($r^2 = 0.974$).

Measurements of the heat flux through the water to the ice surface compared favourably with the laboratory results of

97

Lunardini et al. (1986) except for periods of high wind speed. If water temperature is known, this relationship can be used to estimate the ice melt rate. An alternative approach using the effective thermal diffusivity model can be used to determine ice melt as well. However, additional information is required to refine the empirical relationship between water depth, wind speed and effective thermal diffusivity.

98

REFERENCES

Adams, W.P. (1981) "Snow and Ice on Lakes" in D.M. Gray and G.H. Male (eds) Handbook of Snow, Pergamon Press, Toronto pp.437-474.

Adrian, R.J. (1975) "Turbulent Convection in water over ice" Journal of Fluid Mechanics, Vol. 69, No.4 pp. 753-781.

Andreas, E.L. (1982) "Sensible and Latent heat fluxes and humidity profiles following a step change in surface moisture" CRREL Report, #82-12, pp. 18.

Andreas, E.L. and S.F. Ackley (1982) "On the difference in ablation seasons of Arctic and Antarctic sea ice" CRREL Report, #82-33, pp. 1-9.

Arya, S.P. (1987) Introduction to Micrometeorology. San Diego: Academic Press Incorporated. pp. 307.

Ashton, G.D. (1983) " The decay of ice" Cold Regions Science and Technology, Vol. 8, No.1 pp. 83-86.

Ashton, G.D. (1984) "Deterioration of floating ice covers" in V.J. Lunardi (ed), Proceedings Third International Offshore Mechanics and Arctic Engineering Symposium, A.S.M.E. pp. 26-33.

Ashton, G.D. (1986) River and Lake Ice Engineering. Water Resources Publication, Book Crafters Inc. Chelsea Michigan. pp. 485.

Aver'yanov, V.G. (1983) "The energy-balance structure of the Antarctic ice sheet/atmosphere system as an index of Antarctic Glaciation" Journal of Glaciology, Vol. 29, No. 102 pp. 240-249.

Bilello, M.A. (1969) "Relationship between climate and regional variations in snowcover density in North America" CRREL Report #267, 20 p.

Bilello, M.A. (1980) " Maximum thickness and subsequent decay of lake, river and fast sea ice in Canada and Alaska" CRREL Report #80-6, 120 p.

Boslenga, S.J. (1977) " Preliminary observations on the daily variation of ice albedo" GLERL Contribution No. 84. Great Lakes Environmental Research Laboratory, National Oceanic and Atmosphere Administration., Ann Arbor, Michigan.

Bolsenga, S.J. (1981) "Radiation transmittance through lake ice in the 400-700 nm range" Journal of Glaciology, Vol. 27 No.95, pp 57-66.

Boslenga, S.J. (1988) "Nearshore Great Lakes Ice cover", Cold Regions Science and Technology, Vol. 15 pp. 99-105.

Braithwaite, R.J. (1981) "On glacier energy balance, ablation, and air temperature" Journal of Glaciology, Vol. 27, No. 97 pp. 381-391.

Chorley, R.J. (1962) "Geomorphology and General Systems Theory" Geological Survey Professional Paper 500-B, United States Government Printing Office, Washington, B1-B10.

Clark, W.A.V. and P.L Hosking (1986) Statistical Methods for Geographers, John Wiley and Sons, New York, pp.518.

Colbeck, S.C. (1972) "A theory of water percolation in snow" Journal of Glaciology, Vol. 11 No.63, pp. 369-385.

Colbeck, S.C. (1974) "The capillary effects on water percolation in homogeneous snow" Journal of Glaciology, Vol. 13 No.67 pp. 85-97.

Dilley, A.C. (1968) "On the computer calculation of vapour pressure and specific humidity gradients from psychometric data" Journal of Applied Meteorology, Vol. 7, pp. 717-719.

Fertuck, L.J and J.W. Spyker, W.H.W. Husband (1971) "Numerical estimation of air temperature, wind speed and snow cover" Canadian Society of Mechanical Engineering Transactions, The Engineering Journal, Vol. 14 I-II.

Fox, P.M., J.D. LaPerriere and R.F. Carlson (1979) "Northern Lake Modelling: A literature Review" Water Resource Research, Vol. 4 No.2, pp. 1065-1072.

Gosink, J.P. (1987) "Northern Lake and Reservoir Modelling" Cold Regions Science and Technology, Vol. 13 pp. 281-300.

Granger R.J. and D.H. Male (1978) "Melting of a Prairie Snowpack" _Journal of Applied Meteorology_, Vol. 17 pp. 1833-1842.

Greene G.M. and S.I. Outcalt (1985) " A simulation model of river ice cover thermodynamics" _Cold Regions Science and Technology_, Vol. 10 pp. 251-262.

Hay, J.E and B.B. Fitzharris (1988) "A comparison of the energy-balance and bulk-aerodynamic approaches for estimating glacier melt" _Journal of Glaciology_, Vol. 34 No.177, pp. 145-153.

Henderson-Sellers, B. (1986) "Calculating the surface energy balance for lake and reservoir modelling: a review" _Reviews of Geophysics_, Vol. 24 No.3, pp. 625-649.

Heron, R. (1985) _Decay of a High Arctic Lake Ice Cover_, Ph.D Thesis, McMaster University, p. 189.

Heron, R, and M-K Woo. (1978) "Snowmelt computations for a high arctic site", _Proceedings of the 35th Eastern Snow Conference_, Hanover, New Hampshire, pp.162-172.

Hydrological Atlas of Canada (1978) Ministry of the Environment and Fisheries, Ottawa Canada p. 19.

Langham, E.J. (1981) "Physics and properties of snowcover" in D.M. Gray and D.H. Male (eds) _Handbook of Snow_ Pergamon Press, Toronto. pp. 275-337.

Langleben, M.P. (1968) " Albedo measurements of an arctic ice cover from high towers" _Journal of Glaciology_, Vol. 7, No.50 pp. 289-297.

Langleben, M.P. (1972) " The decay of an annual cover of sea ice" _Journal of Glaciology_, Vol. 11, No.63 pp. 337-344.

Lunardini, V.J., J.R. Zisson and Y.C. Yen (1986) "Experimental determination of heat transfer coefficients in water flowing over a horizontal ice sheet" _CRREL Report_ #86-3 pp. 1-34.

Male, D.H. and D.M. Gray (1981) "Snowcover ablation and runoff" in D.M. Gray and D.H. Male (eds) _Handbook of Snow_ Pergamon Press, Toronto pp. 360-436.

Marsh, P. (1982) <u>Ripening Processes and Meltwater Movement in Arctic Snowpacks</u>, Ph.D. Thesis, McMaster University pp. 178.

Maykut, G.A. and N. Untersteiner (1971) " Some results from a time-dependent thermodynamic model of sea ice" <u>Journal of Geophysical Research</u>, Vol. 76, No.6 pp. 1550-1575.

Moore, D.R. (1983) "On the use of bulk aerodynamic formula over melting snow" <u>Nordic Hydrology</u>, pp. 193-206.

Moore, D.R. and N.O. Weiss (1973) "Non-linear penetrative convection" <u>Journal of Fluid Mechanics</u>, Vol. 25, No.4 pp. 150-156.

Munro, D.S. (1990) "Comparison of lake energy computations and ablatometer measurements on melting ice and snow" <u>Arctic and Alpine Research</u> Vol. 22, No.2 pp. 153-162.

Musman, S. (1968) "Penetrative Convection" <u>Journal of Fluid Mechanics</u>, Vol. 31, No. 2 pp. 343-360.

Myrup, L., D. Gross., L.S. Hoo., and W. Goddard (1970) "Upside-down convection" <u>Weather</u>, Vol. 25, No. 4 pp. 150-156.

Oke, T.R. (1987) <u>Boundary Layer Climate</u> (2nd Edition), Muthuen: London and New York 435 p.

Paterson, W.S.B. (1981) <u>The Physics of Glaciers</u> (2nd Edition), Oxford, Pergamon Press (Pergamon International Library).

Pivovarov, A.A. (1972) <u>Thermal Conditions in Freezing Lakes and Rivers</u>, (Israel Program for Scientific Translations), John Wiley and Sons, New York. pp. 136.

Price, A.J., T. Dunne., and S.C. Colbeck (1976) "Energy Balance and runoff from a sub-arctic snowpack" <u>CRREL Report</u> #76-26, 29 p.

Rumer, R.R. and P.M. Yu (1978) "Modelling ice dissipation in Eastern Lake Erie" <u>Journal of Great Lakes Research</u>, Vol. 4, No.2 pp. 194-200.

Sahlberg, J. (1988) "Modelling the thermal regime of a Lake during the Winter Season" <u>Cold Regions Science and Technology</u>, Vol. 15 pp. 151-159.

Shaw, J.B. (1965) "Growth and Decay of lake ice in the vicinity of Shefferville (Knob Lake), Quebec" Journal of Arctic Institute of North America, Vol. 8, No.2 pp. 123-132.

Thorsteinsson, R. and J. Wm. Kerr (1969) "Cornwallis Island and adjacent smaller island, Canadian Arctic Archipelago" Geological Survey of Canada, Paper Number 67-64 pp. 1-16.

Townsend, A.A. (1964) " Natural convection in water over an ice surface" Quarterly Journal of the Royal Meteorological Society, Vol. 90 pp. 248-259.

Untersteiner, N. (1961) "On the mass and heat budget of arctic sea ice" Archives for Meteorology, Geophysics and Bioclimatology, Vol. A 12, pp. 151-182.

Viskanta, R. and J.S. Toor (1972) " Radiant energy transfer in water" Water Resources Research, Vol. 8, No.3 pp. 595-608.

Wake, A. and R.R. Rumer (1979) " Effect of surface meltwater accumulation on the dissipation of lake ice" Water Resources Research, Vol. 15, No.2 pp. 430-434.

Whittow, J.B. (1984) Dictionary of Physical Geography, Penguin Books, London England, pp. 591.

Williams, G.P. (1957) "An analysis of snow cover characteristics at Aklavick and Resolute, Northwest Territories" National Research Council Canada, Division Building Research, Research Paper 4.

Williams, G.P. (1965) "Correlating freeze-up and break-up with weather conditions, Canadian Geotechnical Journal, Vol. 2, No. 4, pp. 313-326.

Williams, G.P. (1971) " Predicting the date of lake ice breakup" Water Resource Research, Vol. 7, No. 2 pp. 323-333.

Woo, M-K and R. Heron (1981) "Occurrence of ice layers at the base of high arctic snowpacks" Arctic and Alpine Research, Vol. 13, No.2 pp. 225-230.

Woo, M-K., R. Heron and P. Marsh (1981) "Basal ice layers of very cold arctic snowpacks" Proceedings of Eastern Snow Conference, 38 Annual Meeting, Syracuse N.Y. pp. 67-75.

Woo, M-K., R. Heron and P. Marsh (1982) "Basal ice in high arctic snowpacks" Arctic and Alpine Research, Vol. 13, No.2 pp. 225-230.

Woo, M-K and P. Marsh (1978) "Analysis of error in the determination of snow storage for small high arctic basins" Journal of Applied Meteorology, Vol. 17, pp. 1537-1541.

Yen, Y-C. (1968) " Onset of convection in a layer of water formed by melting ice from below" The Physics of Fluids, Vol. 11, No.6 pp. 1263-1270.

Yen, Y-C. (1980) " Free convection heat transfer characteristics in a melt water layer" Transactions of the American Society of Mechanical Engineers, Vol. 102 pp. 550-556.

Yen, Y-C. and F. Galea (1969) " Onset of convection in a water layer formed continuously by melting ice" The Physics of Fluids, Vol. 12, No. 3 pp. 509-516.

105

VITA AUCTORIS

Author: Mr. Emmanuele Mario Novelletto

Date of Birth: May 22, 1966.

Place of Birth: Windsor, Ontario.

Education: Assumption College High School   (1980-1985)

:   University of Windsor (1985-1987)
    Windsor, Ontario.

:   University of Guelph   (1987-1990)
    Guelph, Ontario.
    Honours Bachelor of Science Physical
    Geography (B.Sc.)

:   University of Windsor   (1990-1992)
    Windsor, Ontario.
    Master of Arts Geography (M.A.)

Present Studies: Dalhousie University   (1992-1993)
                 Halifax, Nova Scotia
                 Bachelor of Education (B.Ed.)